Title

An Antimicrobial Peptide and Its Neuronal Receptor Regulate Dendrite Degeneration in Aging and Infection

Journal

Neuron, 97(1)

ISSN

0896-6273

Authors

E, Lezi
Zhou, Ting
Koh, Sehwon
et al.

Publication Date

2018

DOI

10.1016/j.neuron.2017.12.001

Peer reviewed

Published in final edited form as:

Neuron. 2018 January 03; 97(1): 125–138.e5. doi:10.1016/j.neuron.2017.12.001.

An antimicrobial peptide and its neuronal receptor regulate dendrite degeneration in aging and infection

E Lezi[1], **Ting Zhou**[1], **Sehwon Koh**[2], **Marian Chuang**[3], **Ruchira Sharma**[1], **Nathalie Pujol**[4], **Andrew D. Chisholm**[3], **Cagla Eroglu**[2,5], **Hiroaki Matsunami**[1,5], and **Dong Yan**[1,5,*]

[1]Department of Molecular Genetics and Microbiology, Duke University Medical Center, Durham, North Carolina, 27710, USA

[2]Department of Cell Biology, Duke University Medical Center, Durham, North Carolina, 27710, USA

[3]Section of Neurobiology and Cell and Developmental Biology, Division of Biological Sciences, University of California, San Diego, La Jolla, California, 92093, USA

[4]Centre d'Immunologie de Marseille-Luminy, CIML, Aix Marseille Université, Inserm, CNRS, Marseille, 13288, France

[5]Department of Neurobiology and Duke Institute for Brain Sciences, Duke University Medical Center, Durham, North Carolina, 27710,USA

Summary

Infections have been identified as possible risk factors for aging-related neurodegenerative diseases, but it remains unclear whether infection-related immune molecules have a causative role in neurodegeneration during aging. Here, we reveal an unexpected role of an epidermally-expressed antimicrobial peptide, NLP-29 (neuropeptide-like protein 29), in triggering aging-associated dendrite degeneration in *C. elegans*. The age-dependent increase of *nlp-29* expression is regulated by the epidermal *tir-1*/SARM – *pmk-1*/p38 MAPK innate immunity pathway. We further identify an orphan G protein-coupled receptor NPR-12 (neuropeptide receptor 12) acting in neurons as a receptor for NLP-29, and demonstrate that the autophagic machinery is involved cell-autonomously downstream of NPR-12 to transduce degeneration signals. Finally, we show that fungal infections cause dendrite degeneration using a similar mechanism as in aging, through NLP-29, NPR-12 and autophagy. Our findings reveal an important causative role of antimicrobial

[*]Corresponding author/Lead contact: dong.yan@duke.edu, Tel: 919-684-1929, Fax: 919-684-6033.

Author Contributions

L.E and D.Y. devised the whole project. L.E characterized PVD/FLP/PLM dendrite degeneration models and performed all molecular, genetic and imaging experiments. T.Z. and H.M. designed the *in vitro* analysis of the NLP-29 receptor NPR-12. T.Z. performed the calcium imaging experiment in HEK293T cells and analyzed the data with assistance from R.S. and L.E. S.K. and C.E. designed and carried out experiments in cultured rat cortical neurons. M.C., N.P. and A.D.C. provided reagents and shared unpublished results. L.E and D.Y. wrote the manuscript with inputs from all authors.

Competing financial interests

The authors declare no competing financial interests.

peptides, their neuronal receptors and the autophagy pathway in aging- and infection-associated dendrite degeneration.

Keywords

Antimicrobial peptide (AMP); G protein-coupled receptor (GPCR); aging; dendrite degeneration; autophagy

Introduction

Neurons have reciprocal regulatory interactions with surrounding cells. The innate immune system, as well as many molecules with immune functions, plays important roles in the nervous system (Boulanger, 2009; Stephan et al., 2012). Recent studies show that the dramatic increase of C1q, the pattern recognition molecule of the classical complement cascade that functions in the innate immune system to remove pathogens upon infections, triggers the functional aging of the brain (Sekar et al., 2016; Stephan et al., 2013). While the reason for the increased expression of such immune molecules in the aging brain is still unknown, studies have implicated that sporadic Alzheimer's disease (AD) is associated with infections by pathogenic microbes, such as fungi, herpes simplex virus and pneumonia-causing *Chlamydophila pneumonia* (Hill et al., 2014). However, it remains unclear whether infections cause the degeneration of neurons, and whether any immune molecules that can be induced by infections contribute to aging-associated neurodegeneration.

Antimicrobial peptides (AMP) are host defense peptides, and play important roles in fighting microbe pathogens after infections (Zhang and Gallo, 2016). Emerging evidence shows that some AMPs are highly expressed in mouse microglia (Hickman et al., 2013) as well as in the astrocytes of AD patients' brains (Williams et al., 2013) despite the absence of infection, suggesting that AMPs may have non-antimicrobial functions in the nervous system.

Dendrite and axon degeneration occur in both normal aging and aging-related neurodegenerative diseases, and are considered major causes of neuronal dysfunction (Adalbert and Coleman, 2013; Dickstein et al., 2007; Lin and Koleske, 2010). Studies have revealed factors involved in the regulation of axon degeneration (Wang et al., 2012), while the mechanisms underlying dendrite degeneration remain largely unknown.

Here, using *C. elegans* PVD neurons as a model, we show that aging-associated expression of NLP-29 (neuropeptide-like protein 29), an epidermally-expressed AMP (Couillault et al., 2004; Pujol et al., 2008a), causes dendrite degeneration. We further identify a conserved orphan G protein-coupled receptor (GPCR) NPR-12 (neuropeptide receptor 12) as the receptor in neurons for NLP-29, and show that NPR-12 signaling induces autophagy to mediate aging-associated dendrite degeneration. Moreover, we find that fungal infections can induce dendrite degeneration through the same mechanism as in aging. Finally, we present evidence to show that NLP-29/AMP can cause dendrite degeneration in NPR-12-expressing rat cortical neurons through the autophagic machinery as well, suggesting that the finding we report here is likely to be evolutionarily conserved. Therefore, our study

uncovers an unexpected novel function of NLP-29/AMP and its neuronal receptor in regulating dendrite degeneration, and provides a new mechanism for dendrite degeneration in physiological and pathological conditions.

Results

PVD neurons exhibit aging-associated dendrite degeneration

To investigate aging-associated neurodegeneration *in vivo*, we used *C. elegans* PVD neurons as a model. Each of the two PVD neurons, PVDL and PVDR, has extensive, highly-branched and well-organized dendritic arbors, with one ventrally oriented axon (Fig. 1A) (Smith et al., 2010). First, we characterized the PVD degeneration pattern during aging by observing the changes of dendrite morphology in control animals [*wdIs51*(*F49H12.4::GFP*)] from Day 1 to Day 9 of adulthood consecutively, with Day 1 defined as 24 hours after the final larval stage (L4). Progressive dendrite morphological changes were observed in these animals over the course of aging (Fig. 1A). Specifically, the PVD dendrites developed bead or bubble-like structures along dendrites and were enriched in autophagosomes (Fig. 1B), which is similar to what was observed in mammalian neurons of neurodegenerative disease models (Menzies et al., 2015). Cytoskeleton disorganization, such as microtubule instability, has been well documented in neurodegeneration (Wang and Mandelkow, 2016). We next examined the distribution of polymerized microtubules in PVD dendrites using EMTB::GFP (Richardson et al., 2014), and observed fragmented and discontinued microtubule filaments in aged but not young animals (Fig. S1D). Interestingly, most of these fragmented EMTB::GFP signals appeared to be enriched in the aging-associated bead/bubble-like structures (Fig. S1D). While PVD dendrites underwent progressive morphological changes over the course of aging, PVD axons and cell bodies did not display significant bead or bubble-like structures within the same time frame (Fig. S1A–B). The distributions of axonal autophagosomes and microtubules were also similar in young and aged animals (Fig. S1C and S1D).

For quantification of age-dependent PVD dendritic morphological change, an animal was considered as having such change if a total of ten or more bead or bubble-like structures were observed in more than five PVD functional units (dendritic menorahs) (Oren-Suissa et al., 2010). The number of control animals with dendritic morphological changes significantly increased with age: 30 % of them started to show bead or bubble-like structures on Day 5 of adulthood, 50 % on Day 6, and almost 100 % on Day 7 (Fig. 1C), while the onset of dendritic morphological changes in these animals preceded animal death by several days (Fig. 1C). In addition, there was an age-dependent progressive increase in the severity of dendritic morphological changes, quantified as the number of bead or bubble-like structures in each control animal (Fig. 1D). Next, we tested whether the morphological changes of PVD dendrites were accompanied by any alteration in PVD function. PVD neurons are responsible for the response to harsh touch applied to the mid-part of the body, where the animal subsequently initiates forward or backward movements (Chatzigeorgiou et al., 2010; Li et al., 2011; Way and Chalfie, 1989). Activating the touch receptor neurons, including ALM, AVM, PLM, and PVM, by gentle touch can also generate similar behavioral responses (Way and Chalfie, 1989). To exclude the possible effects of the touch receptor

neurons in our behavioral tests, we assessed PVD function in a *mec-4* mutant background, which lacks functioning touch receptor neurons but has normally-functioning PVD neurons (Driscoll and Chalfie, 1991) (Liu and Shen, 2012). We used *mec-3* mutants, which have dysfunctions in both PVD and touch receptor neurons, as a positive control for the 'no harsh touch response' (Way and Chalfie, 1989). Consistent with previous observations, approximately 60 % of *mec-3* mutants did not respond to harsh touch (Liu and Shen, 2012), a fraction that was consistent over Day 1–10 (Fig. 1E). On the other hand, *mec-4* animals, considered to have wild-type responses to harsh touch, showed an age-dependent increase in the 'non-response rate' (Fig. 1E), which mirrored the observed PVD morphological changes (bead or bubble-like structures).

Neurodegeneration is defined as a progressive loss of neurons or their processes (axons and dendrites) with a corresponding progressive impairment in neuronal function (Jack et al., 2013). Although we did not observe a loss of PVD dendritic menorahs in the time frame we examined (Fig. S1E), the bead or bubble-like structures along PVD dendrites, which were enriched with autophagosomes and fragmented microtubules, demonstrated the features of neurodegeneration. Similar beading or blebbing of neurites has been used as a marker of neurodegeneration in both invertebrate and vertebrate models (Kuchibhotla et al., 2008; Morsch et al., 2015; Pan et al., 2011). Moreover, PVD neurons underwent an aging-associated functional decline that coincided temporally with the morphological changes of their dendrites (Fig. 1E). Based on these evidence, we conclude that PVD neurons display aging-associated dendrite degeneration at both morphological and functional levels. We thus characterized PVD dendrite degeneration by bead or bubble-like structures formed along the dendrites, and an animal was considered to exhibit PVD dendrite degeneration when a total of ten or more bead or bubble-like structures were observed in more than five dendritic menorahs (See more details in the Method section). Given that PVD axons and cell bodies did not show noticeable morphological and structural changes within the same time period (Fig. S1A–D), the dendrite degeneration we observed was likely to represent the early stage of PVD neurodegeneration.

To further demonstrate that the PVD dendrite degeneration we describe here is associated with aging, we tested whether changing animal lifespan could alter this phenotype. Loss-of-function (*lf*) in *daf-2*, the insulin/IGF receptor, can greatly extend the lifespan of *C. elegans* (Apfeld and Kenyon, 1998). Consistent with the essential role of *daf-2* in aging, we found that a *daf-2(lf)* mutation significantly delayed the onset of aging-associated PVD dendrite degeneration (Figure S1F). *daf-2* appeared to regulate aging-associated degeneration in a non-cell-autonomous manner (Figure S1F), similar to its non-cell-autonomous functions in regulating lifespan (Apfeld and Kenyon, 1998). These data further support that the PVD dendrite degeneration phenotype we show here is aging-associated.

Epidermal NLP-29/AMP triggers aging-associated PVD dendrite degeneration

Through a genetic screen, we found that a loss-of-function *(lf)* mutation *(tm1931)* in *nlp-29* significantly delayed the onset of aging-associated PVD dendrite degeneration at both morphological and functional levels (Fig. 2A–2D, S1B), while *nlp*-29*(tm1931)* animals had a comparable lifespan to that of control animals (Fig. S2A). To further confirm our

observation, we generated a second *lf* allele, *nlp-29(yad90)*, in which the coding region of *nlp-29* was deleted (Fig. S3A). *nlp-29(yad90)* delayed aging-associated PVD dendrite degeneration to the same degree as observed in *nlp-29(tm1931)* (Fig. 2B). Expression of NLP-29::GFP under its own promoter with its own 3′UTR fully rescued *nlp-29(tm1931)* phenotypes (Fig. 2E). *nlp-29* is mainly expressed in the epidermis, and functions as an AMP to combat infection via the skin (Couillault et al., 2004). We found that RNAi knock-down of *nlp-29* in the epidermis was sufficient to delay aging-associated PVD dendrite degeneration as in *nlp-29(lf)* mutants, while PVD-specific knock-down of *nlp-29* did not cause any obvious delay of dendrite degeneration (Fig. S3C). Consistent with these results, expression of *nlp-29* using an adult epidermis-specific promoter (*Pcol-19*) was able to rescue *nlp-29(tm1931)* phenotypes (Fig. 2E). With these observations, we conclude that epidermally-expressed *nlp-29* plays a key role in regulating aging-associated PVD dendrite degeneration.

To further confirm the essential role of NLP-29 in PVD dendrite degeneration, we microinjected synthetic NLP-29 peptide into control animals at Day 1 at 10 μM and 100 μM (Fig. 3A). As a control peptide, we used a highly similar AMP NLP-31 at 100 μM (Fig. S3B). At 24 hours post injection (Day 2), approximately 45 % of animals injected with 10 μM NLP-29 and 60 % injected with 100 μM NLP-29 displayed PVD dendrite degeneration, while only ~25% injected with vehicle (DMSO) or NLP-31 showed dendrite degeneration (Fig. 3A). Similar to what was observed during aging-associated degeneration, we found that autophagosomes were also enriched in degenerating PVD dendrites of NLP-29-injected animals (Fig. S3F), while similar injections did not cause any obvious changes in PVD axons (Fig. S3E–F). In addition, we observed that epidermis-specific overexpression of *nlp-29* induced an early onset of aging-associated PVD dendrite degeneration (Fig. 3B). These data show that overproduction of NLP-29 is sufficient to induce PVD dendrite degeneration.

Our results led us to hypothesize that aging-associated PVD dendrite degeneration is triggered by age-dependent changes in *nlp-29* expression level. Indeed, both *nlp-29* mRNA and protein levels increased with age in control animals (Fig. 3C–D and Fig. S3D), and the significant increase of *nlp-29* expression on Day 5 coincided temporally with the dramatic increase in the number of animals with PVD dendrite degeneration over the course of aging. The age-dependent change in epidermal *nlp-29* expression was also confirmed by an increase in the number of control animals [*nlp-29* transcriptional reporter: *frIs7(Pnlp-29::GFP; Pcol-12::dsRed)* (Pujol et al., 2008a)] with *Pnlp-29::GFP* induction during aging (Fig. 3E).

As *C. elegans* age, the skin displays structural changes such as thickened cuticles and thinner epidermis (Herndon et al., 2002), which could potentially lead to a loss of epidermal integrity and subject aged animals to a higher susceptibility to microbial infections. Under lab culture conditions, *C. elegans* uses *E. coli* OP50 as a food source. As OP50 can be pathogenic to older *C. elegans* (Garigan et al., 2002), one may argue that changes in epidermal integrity or microbial infections could contribute to the age-dependent increase of *nlp-29* expression and PVD dendrite degeneration that we observed. To test these possibilities, we first examined the epidermal integrity using Hoechst 33258 as previously

described (Moribe et al., 2004). By counting the percentage of animals with staining of epidermal nuclei, we found that there was no significant difference in epidermal integrity between Day 1 and Day 7 control animals (Fig. S2B–C). Also, none of the mutations examined in this study seemed to affect epidermal integrity (Fig. S2B–C). We further showed that aging-associated PVD dendrite degeneration was unlikely to be associated with microbial infections, as animals grown on dead (heat-killed) OP50 or plates supplemented with anti-fungal drugs (nystatin or amphotericin B) displayed age-dependent *Pnlp-29::GFP* induction and PVD dendrite degeneration to a similar extent as in animals grown under control conditions (Fig. 3E–3H).

During infection, the expression level of *nlp-29* is regulated by a conserved innate immune signaling cascade in the epidermis, consisting of TIR-1/SARM, NSY-1/MAP3K, SEK-1/MAP2K and PMK-1/p38 MAPK (Dierking et al., 2011; Labed et al., 2012; Pujol et al., 2008a). We found that loss of function in *pmk-1* or *tir-1* also delayed aging-associated PVD dendrite degeneration (Fig. S4A). Double mutants of *nlp-29* with *tir-1* or *pmk-1* did not show a stronger delaying effect when compared to *nlp-29(lf)* single mutants, suggesting that *tir-1*, *pmk-1* and *nlp-29* lie within the same pathway to influence aging-associated PVD dendrite degeneration (Fig. S4B). A previous study showed that TIR-1 and PMK-1 could function in neurons to regulate neurodegeneration in a *C. elegans* amyotrophic lateral sclerosis model (Veriepe et al., 2015). We examined the potential neuronal functions of TIR-1 and PMK-1 in aging-associated PVD dendrite degeneration by tissue-specific RNAi. PVD-specific knock-down of TIR-1 or PMK-1 did not affect the onset of PVD dendrite degeneration, while knock-down of TIR-1 or PMK-1 in the epidermis delayed PVD dendrite degeneration [Fig. S4C (epidermis RNAi) and Fig. S4D (PVD RNAi)]. These results confirm that the TIR-1-PMK-1 pathway functions in the epidermis, but not in neurons, and does this via controlling *nlp-29* expression to regulate PVD dendrite degeneration.

NLP-29 activates NPR-12, a neuronal GPCR, to regulate PVD dendrite degeneration

PVD dendrites are anatomically sandwiched between the epidermis and body wall muscle (Albeg et al., 2011). One possibility for how epidermal NLP-29, a small peptide, may communicate with PVD dendrites is through ligand-receptor binding. NLP-29 was initially identified and named for its sequence similarity with YGGWamide neuropeptides (Nathoo et al., 2001). We hypothesized that the potential neuronal receptor(s) for NLP-29 might be known or predicted neuropeptide receptors. PVD neurons express at least 8 potential neuropeptide receptors: *dmsr-1*, *npr-2*, *npr-12*, *npr-32*, *pdfr-1*, *C17H11.1*, *lat-1* and *T21H3.5* (Frooninckx et al., 2012; Smith et al., 2010). We tested all these receptors and found that two *npr-12(lf)* alleles had aging-associated PVD dendrite degeneration patterns comparable to that of *nlp-29* mutants, while mutating or knocking down other neuropeptide receptors did not reproduce the degeneration delaying effect of *nlp-29(lf)* (Fig. 4A–B, S1B and S5A–B). NPR-12, an ortholog of human pyroglutamylated RFamide peptide receptor, is an orphan GPCR predicted to have a neuropeptide Y receptor-like activity (Frooninckx et al., 2012). We confirmed the expression of *npr-12* in PVD neurons, including the cell body, dendrites and axons, using *npr-12* transcriptional and translational reporter strains (*Pnpr-12::GFP, Pnpr-12::NPR-12::GFP*) (Fig. S5C–D). The delayed onset of PVD dendrite degeneration in *npr-12* mutants was also accompanied by a delayed onset of aging-associated PVD

dysfunction (Fig. 4C). Unlike *nlp-29*, no age-dependent changes of *npr-12* expression were observed in control animals (Fig. S5E). PVD-specific knock-down of *npr-12* delayed the onset of PVD dendrite degeneration as in *npr-12(lf)* mutants, while epidermis-specific knock-down did not (Fig. S5F). Both ubiquitous and PVD-specific expression of *npr-12* cDNA were able to rescue the PVD dendrite degeneration phenotype in *npr-12*(*tm1498*) mutants to similar extents (Fig. 4D). These results suggest that *npr-12* functions cell-autonomously to regulate PVD dendrite degeneration.

Next, we demonstrated that *nlp-29* and *npr-12* acted in the same genetic pathway by showing that *npr-12;nlp-29* double mutants did not display an enhanced PVD dendrite degeneration delaying effect when compared with the single mutants of *nlp-29* and *npr-12* (Fig. 4E). Moreover, we showed that *npr-12(lf)* blocked PVD dendrite degeneration induced by synthetic NLP-29 peptide microinjected into young adults (Fig. 4F). Similarly, *npr-12(lf)* was also able to suppress the early onset PVD dendrite degeneration induced by epidermal *nlp-29* overexpression (Fig. 4G). Collectively, these evidence indicate that NPR-12 acts downstream of NLP-29.

To test whether NPR-12 is a functional receptor for NLP-29, we transiently transfected HEK293T cells with a plasmid containing *C. elegans npr-12* cDNA. Cell-surface expression of NPR-12 modified with an N-terminal FLAG tag was confirmed by live-cell surface immunochemistry staining (Fig. 4H). NPR-12 is an orphan GPCR, and no previously published information is available regarding its coupled G protein. Therefore, we conducted experiments by co-expressing NPR-12 and the promiscuous G protein Gα15, which couples with many GPCRs and leads to intracellular calcium release when activated (Offermanns and Simon, 1995). We stimulated HEK293T cells transiently expressing NPR-12, Gα15 and GCaMP6s with a perfusion solution containing 10 μM synthetic NLP-29. We found that stimulation of the NPR-12 transfected cells with 10 μM NLP-29 induced a significant elevation of calcium, while the solvent-only control did not cause any changes (Fig. 4I–J and Fig. S6C–G). To further test the specificity of this response, we examined the effect of NLP-29 on NPR-32, another GPCR expressed in PVD neurons, and the human beta2-adrenergic receptor (β2-AR), also a GPCR. In this assay, NLP-29 failed to elicit a significant response in NPR-32- or β2-AR-expressing cells (Fig. 4I–J, and Fig. S6A–B and Fig. S6I–P). We stimulated NPR-12-expressing cells with NLP-31, an AMP closely related to NLP-29 in *C. elegans*, and no response was observed either (Fig. 4I–J, and Fig. S6H). Altogether, through genetic analysis of *npr-12(lf)* phenotypes, functional analysis of *npr-12(lf)'s* ability to suppress NLP-29-induced PVD dendrite degeneration, and examination of ligand-receptor interactions *in vitro*, we conclude that NPR-12 is the receptor for NLP-29 in mediating aging-associated PVD dendrite degeneration.

Autophagic machinery acts downstream of NPR-12 in PVD dendrite degeneration

Accumulation of autophagosomes and late autophagic vacuoles in the distal dendrites/axons of degenerating neurons has been well documented in mammals (Feng et al., 2017; Yu et al., 2005). As described earlier, we also showed autophagosomes were enriched in degenerating PVD dendrites during aging (Fig. 1B), raising the possibility that activation of NPR-12 may recruit the autophagic machinery to trigger PVD dendrite degeneration. Supporting this

assumption, we found that co-injection of bafilomycin A1 (Baf A1), an autophagy inhibitor (Zhang et al., 2015), was able to suppress the induced-PVD dendrite degeneration in NLP-29 peptide injected animals (Fig. 5A). To further confirm the function of autophagy in aging-associated PVD degeneration, we examined mutants affecting different steps of the autophagy pathway, including *atg-3*, *atg-4.1* and *epg-5*. ATG-4.1 cleaves the ubiquitin-like protein LGG-1 to generate a functional form LGG-1-I that can further conjugate with phosphatidylethanolamine via ATG-3 and other sequential actions to form autophagosomes (Wu et al., 2012). EPG-5 is then subsequently required for the fusion of autophagosomes and lysosomes to form degradative autolysosomes (Lu et al., 2011). As shown in Fig. 5B, mutations in *atg-3*, *atg-4.1* and *epg-5* caused similar delays of PVD dendrite degeneration onset as those in *nlp-29* and *npr-12* mutants. To address the genetic interactions between autophagy, *nlp-29* and *npr-12*, we further analyzed *atg-4.1(lf)* mutants. *atg-4.1(lf)* delayed the aging-associated PVD dendrite degeneration at both morphological and functional levels (Fig. 5B–5D, S1B), while the mutant animals had a comparable lifespan to that of the controls (Fig. S2A). The double mutants *atg-4.1;nlp-29* or *atg-4.1;npr-12* exhibited the same degree of PVD dendrite phenotypes as those in single mutants (Fig. 5E). Also, *atg-4.1(lf)* suppressed the early PVD dendrite degeneration caused by epidermal *nlp-29* overexpression (Fig. 5F). Moreover, PVD-specific rescue of *atg-4.1* could restore the delayed PVD dendrite degeneration in *atg-4.1(lf)* mutants (Fig. 5G). Collectively, these results indicate a cell-autonomous involvement of the autophagic machinery in *nlp-29 – npr-12* regulated PVD dendrite degeneration.

NLP-29 and NPR-12 regulate dendrite degeneration in other *C. elegans* and mammalian neurons

npr-12 is expressed in neurons other than PVD as well (Fig. S5D), such as the head sensory FLP neurons (Albeg et al., 2011). Over the course of aging, FLP dendrites in control animals [*yadEx650* (*Pmec-3::GFP*)] displayed progressive degeneration, and loss-of-function in *nlp-29* and *npr-12* significantly delayed the onset of FLP dendrite degeneration (Fig. 6A–B). Similar to what was observed in PVD neurons, *nlp-29* functioned in the epidermis and *npr-12* acted cell autonomously to regulate FLP dendrite degeneration (Fig. 6B). Next, we examined the degeneration-triggering function of *nlp-29* and *npr-12* in posterior sensory PLM neurons, which do not endogenously express *npr-12*. In control animals, PLM sensory processes/dendrites showed mild to moderate progressive degeneration over the course of aging (Fig. 6C–D), while animals with PLM ectopically expressing *npr-12* had a significantly earlier onset of degeneration (Fig. 6D). Importantly, the *nlp-29(lf)* mutation was able to block this additional effect and bring the degeneration rate back to the control level (Fig. 6D). Furthermore, we tested whether direct access to the epidermis was required for NPR-12 to receive NLP-29 in regulating dendrite degeneration. To do this, *npr-12* was ectopically expressed in amphid sensory neurons, which have dendrites surrounded by glial cells. As shown in Fig. S5G–H, amphid sensory neurons of control animals [*yadEx1037(Parl-13::GFP)*] displayed very slight dendrite degeneration over the course of aging, demonstrated by beading or forming vacuoles along the dendrites. We found that ectopic expression of *npr-12* did not further increase the dendrite degeneration rate in amphid neurons (Fig. S5H), suggesting that direct access to epidermal NLP-29 is likely critical for neuronal NPR-12 to transmit degeneration signals.

In addition, we tested the ability of NLP-29 and NPR-12 in regulating mammalian dendrite degeneration using cultured rat cortical neurons. As shown in Figure 6E, treating NPR-12-expressing cortical neurons with NLP-29 induced significant dendrite degeneration, which appeared gradually over the time with the presence of NLP-29 (Fig. S6Q), while NLP-29 by itself did not show neuronal toxicity (Fig. 6F). Degeneration was not observed in NPR-12-expressing cortical neurons treated with the control peptide NLP-31 (Fig. 6G–H, Fig. S6R). Similar to what was found in *C. elegans* neurons, inhibition of the autophagy pathway with bafilomycin A1 prevented NLP-29/NPR-12-induced degeneration in rat cortical neurons (Fig. 6G–H). Unlike in *C. elegans* neurons, we observed that NLP-29-treated NPR-12-expressing rat cortical neurons not only had bead or bubble-like structures along their dendrites but also a loss of dendritic branching, further supporting the significance of the NLP-29 - NPR-12 - autophagy pathway in regulating neurodegeneration. Although the reason for the lack of dendritic loss in aged *C. elegans* neurons is still unclear, it is possible that some signals involved in dendritic pruning during aging may be absent in nematodes.

Taken together, these results show that NLP-29 and NPR-12 can mediate dendrite degeneration in other *C. elegans* neurons as well as in mammalian neurons, in support of an evolutionarily conserved function of AMPs and their neuronal receptors in regulating dendrite degeneration.

Fungal infection induces dendrite degeneration via NLP-29 and NPR-12

NLP-29 has been characterized as an AMP (Couillault et al., 2004), whereas our study reveals its unexpected role in dendrite degeneration. This raises the question as to whether NLP-29 has functions in both fighting pathogens and inducing dendrite degeneration during infection. To address this question, we infected animals with a nematode fungal pathogen *Drechmeria coniospora*, which is known to trigger an immune response and induce the expression of AMPs including *nlp-29* in *C. elegans* (Pujol et al., 2008b). 36-hour exposure to *Drechmeria coniospora* on Day 1 induced a 6-fold increase of *nlp-29* mRNA expression in control animals, but did not change *npr-12* mRNA expression (Fig. S7B–C). We found that infection of Day 1 animals caused significant PVD dendrite degeneration, while control treatment did not induce any obvious phenotypes (Fig. 7A). Microbe-associated molecular patterns (MAMPs) are molecules associated with certain microbial groups, and can be recognized by hosts to trigger innate immune responses, and in some cases do so without harming the host cells (Chu and Mazmanian, 2013). Although it is not clear whether or which MAMPs can be detected by *C. elegans* (Luallen and Troemel, 2014), we treated control animals with heat-killed *D. coniospora* to exclude the possibility of *D. coniospora*-associated MAMPs causing the dendrite degeneration phenotype. As shown in Fig. S7D–E, 36-hour exposure of heat-killed *D. coniospora* did not increase *nlp-29* expression or cause PVD dendrite degeneration in Day 1 control animals, suggesting that *D. coniospora*-induced PVD degeneration is not associated with MAMP stimulations.

We then found that *nlp-29(lf), npr-12(lf)* and *atg-4.1(lf)* were able to completely block the infection-induced PVD dendrite degeneration (Fig. 7A). Compared to aging-associated degeneration, the rate of degeneration induced by infections is relatively low. This may be due to protective mechanisms in young animals, as infection of older animals caused more

severe phenotypes (Fig. 7B). We also examined whether fungal infection would affect other *C. elegans* neurons. As shown in Figure 7C, in infected animals, FLP dendrites displayed significantly higher degeneration rates when compared to the 'non-infected' group. Furthermore, *nlp-29(lf)* and *npr-12(lf)* mutations blocked the FLP degeneration caused by infection (Fig. 7C). Interestingly, infection did not induce obvious degeneration of PLM dendrites/sensory processes, which did not express *npr-12* endogenously (Fig. 7D). However, ectopic expression of *npr-12* in PLM neurons was sufficient to cause infection-dependent degeneration, while *nlp-29(lf)* substantially suppressed this effect (Fig. 7D). These results suggest that NLP-29 can function in both fighting pathogens and triggering dendrite degeneration, and in dendrite degeneration the function of NLP-29 relies on the expression of its neuronal receptor NPR-12.

Discussion

Using *C. elegans* PVD neurons as a model, we investigate the molecular mechanisms underlying aging- and infection- associated dendrite degeneration. During aging, PVD dendrites display progressive degeneration. As a result, most aged animals lose their responses to harsh touch, a function mediated by PVD neurons. We find that loss-of-function in an epidermally-expressed AMP NLP-29 suppresses the aging-associated PVD dendrite degeneration. Consistent with this finding, the expression level of *nlp-29* is positively correlated with age, and increasing NLP-29 is sufficient to cause PVD dendrite degeneration in young adult animals. Moreover, we identify the GPCR NPR-12 in the PVD neuron as the receptor for NLP-29, and the autophagy pathway acts downstream of NPR-12 in mediating aging-associated PVD dendrite degeneration (Fig. S7I). We further present evidence to show that the NLP-29-NPR-12 regulation is also involved in infection-associated dendrite degeneration. The function of AMPs and their neuronal receptors in dendrite degeneration appears to be evolutionarily conserved, as NLP-29/AMP can trigger dendrite degeneration in NPR-12-expressing rat cortical neurons as well.

Besides the bead/bubble-like structures found in aging PVD dendrites, we also observe age-dependent changes of dendritic organization/branching (Fig. S7F–H). However, these changes appear irrelevant to the functional aging of PVD neurons, as a mutation in *nlp-29*, *npr-12* or *atg-4.1* strongly delays the functional decline of PVD in aging without affecting the aging-associated changes in dendritic organization/branching (Fig. S7G–H). On the other hand, the aging-associated bead or bubble-like structures along dendrites that we observe are tightly linked to the functional aging of PVD neurons. In fact, these structures are also documented in degenerating neurons from fruit flies to rodents as well as in patients with neurodegenerative diseases (Greenwood et al., 2007; Su et al., 1993; Tao and Rolls, 2011); therefore, they appear to be evolutionarily conserved features of neurodegeneration. Although the components/molecular features of the bead or bubble-like structures are still unclear, we show that autophagosomes and fragmented microtubules are enriched in these structures along the dendrites, and the autophagy pathway plays important roles in their formation. Further studies on the mechanisms underlying the induction of such bead/bubble-like structures may provide insights into how neurodegeneration is initiated.

While PVD dendrites undergo progressive aging-associated degeneration over the first 9 days, PVD axons do not show significant degeneration during the same time period, suggesting the aging-associated dendrite and axon degeneration use distinct mechanisms in *C. elegans*. PVD neurons have complex dendritic branches and a single axon; the tertiary and quaternary dendrites are in association with the epidermis (Oren-Suissa et al., 2010), whereas the axons run in the ventral nerve cord and are separated from the epidermal tissues (White et al., 1976, 1986). As NPR-12 is expressed in both PVD dendrites and axons, it seems that epidermally-released NLP-29/AMP can only function locally to affect PVD dendrites, while PVD axons are less affected due to their anatomical position. This conclusion is further supported by the results from examining the degeneration of PLM and amphid sensory neurons. Namely, expression of NPR-12 in epidermis-associated PLM neurons induces NLP-29-dependent aging-associated degeneration, while expression of NPR-12 in amphid neurons, which are not associated with epidermis, did not affect their degeneration. However, injection of NLP-29 in young animals only causes degeneration in the PVD dendrite but not in the axons, suggesting additional protective mechanisms may be involved.

In this study, we show that NLP-29/AMP and its neuronal receptor can function in both aging- and infection- associated dendrite degeneration, which again raises the question as to whether there indeed are connections between infection and the pathogenesis of aging-related neurodegenerative diseases. While the current evidence for such connections remain limited, a classical example of infection-induced neurodegeneration in humans would be HIV-associated dementia, as studies have suggested that direct exposure to HIV-1 or indirect damage through toxic substances released by infected or immune-stimulated microglia and astrocytes may cause neurotoxicity (Kaul et al., 2005). Amyloid beta (Aß) has long been implicated in AD, and its expression level increases with age in cognitively intact human subjects as well (Lesne et al., 2013). Recent studies have demonstrated that soluble Aß oligomers can bind to microbes, functioning as AMPs (Kumar et al., 2016). Given these parallels between NLP-29 and Aß, our data further provide mechanistic evidence for infection-related AMPs mediating neurodegeneration during aging.

The essential function of epidermally-expressed AMP NLP-29 in neurodegeneration we report here reveals a critical role of epidermal cells in regulating neuronal aging, which joins emerging evidence of non-cell-autonomous mechanisms of neurodegeneration (Garden and La Spada, 2012; Ilieva et al., 2009). The epidermis is considered to function as the skin of *C. elegans*, but recent studies also show that epidermal cells can play similar roles as glial cells/neuronal support cells to regulate dendrite development, synapse formation, and neuronal activity (Dong et al., 2013; Salzberg et al., 2013; Shao et al., 2013; Stawicki et al., 2011). Glial cells/neuronal support cells have been implicated in the pathogenesis of neurodegenerative diseases. Interestingly, some AMPs are highly expressed in mouse microglia (Hickman et al., 2013) and astrocytes of AD patients (Williams et al., 2013) in the absence of infections. Therefore, the AMP mediated non-cell-autonomous signaling from neuronal support cells may be evolutionarily conserved for neuronal aging.

STAR Methods

Contact for Reagent and Resource Sharing

Further information and requests for resources and reagents should be directed to and will be fulfilled by the Lead Contact, Dong Yan (dong.yan@duke.edu).

Experimental Model and Subject Details

C. elegans* Strains and Maintenance—C. elegans* strains were maintained on NGM plates at 20 °C as described previously (Brenner, 1974), and only hermaphrodites were used for experiments. For all aging-associated experiments, adults were bleach treated to kill possible pathogenic microbes and to yield age-synchronized animals. Then hermaphrodites of L4 stage were picked and grown on NGM plates with 5′-flurodeoxyuridine (FUDR) to inhibit progeny growth. Day 1 adulthood was defined as in 24 hours after L4 stage. Dead *E. Coli* OP50 was prepared by heating at 100 °C for 30 min. For experiments with anti-fungal dru gs, 10 μg/mL (final concentration) nystatin or 1.6 μg/mL (final concentration) amphotericin B was supplemented in NGM plates. All transgenes and strains are described in Table S1. *nlp-29(yad90)* allele was generated using CRISPR by co-injecting plasmids expressing two probes: CAGGAGGATATGGAGGATA and TCCATATCCCCATTGTGCGC.

Cell Cultures—HEK293T cells were maintained in minimal essential medium (Sigma) containing 10 % fetal bovine serum (Sigma) with penicillin-streptomycin and amphotericin B. Rat cortical neurons were purified from postnatal day 1 Sprague-Dawley rat pups (Charles River Laboratories) of both sexes by sequential immunopanning and cultured in serum-free medium containing BDNF, CNTF, and forskolin on laminin-coated coverslips as previously described (Risher et al., 2014). All experiments were conducted in accordance with the Duke University Institutional Animal Care and Use Committee guidelines (IACUC Protocol Numbers A173-14-07 and A147-17-06).

Method Details

DNA Constructs and Generation of Transgenes—All DNA expression constructs were made using Gateway cloning technology (Invitrogen). Sequences of the final clones were confirmed. The information for each construct is in Table SI. Primer sequences are available upon request. Transgenic animals were generated following standard procedures (Mello et al., 1991). In general, plasmid DNAs of interest were used at 10–100ng/ml with the co-injection marker *Pttx-3::RFP* or *Pttx-3::GFP* at 50ng/ml. For each construct, two to five independent transgenic lines were analyzed. Table SI lists genotypes and DNA constructs for transgenes.

Transfection—HEK293T cells were plated on poly-D-lysine-coated 35 mm glass-bottom dish (MatTek) and transfected with plasmids coding for GCaMP6s, mouse Gα15, along with FLAG-NPR-12, FLAG-NPR-32 or human β2-AR using Lipofectamine 2000 (Invitrogen).

The rat cortical neurons were transfected using the Lipofectamine LTX (Invitrogen) reagent on days *in vitro* 6 (DIV6) with plasmids coding NPR-12-2A-GFP or GFP only. At DIV 9,

the transfected neurons were treated with NLP-29 or NLP-31 peptide at 10 μM final concentration, and the peptides were present in the culture thereafter for 3 days.

Fluorescence Microscopy—We scored fluorescent reporters in live animals using a Zeiss Axio Imager 2 microscope equipped with Chroma HQ filters. Confocal images were collected of animals immobilized by 1 % 1-phenoxy-2-propanol (TCI America) in M9 buffer using a Zeiss LSM700 confocal microscope. Pictures shown in the figures are projections of z-stack images (1 μm/section). GFP-expressing rat cortical neurons were imaged at DIV 12 with Zeiss Axioimager M1 Epifluorescence Microscope (Carl Zeiss) using a 20X objective.

Quantification of Dendrite Degeneration—In this study, dendrite degeneration in *C. elegans* was characterized as bead or bubble-like structures along the neuron processes, and was quantified under 63X magnification. *wdIs51 (F49H12.4::GFP)* (Smith et al., 2010), *zdIs5 (Pmec-4::GFP)* (Clark and Chiu, 2003), and *yadEx650 (Pmec-3::GFP)* were used to visualize PVD, PLM, and FLP neurons, respectively. An animal was considered to be undergoing PVD dendrite degeneration if a total of ten or more bead or bubble-like structures were observed in more than five PVD functional units (menorahs) (Oren-Suissa et al., 2010). For the severity of PVD dendrite degeneration, the number of bead or bubble-like structures along PVD dendrites (the entire dendritic tree of either PVDL or PVDR) was counted for each animal. An animal was considered to be undergoing FLP dendrite degeneration if five or more bead or bubble-like structures were observed along the dendrites. For PLM neurodegeneration, the quantification was focused on anterior processes/dendrites. An animal was considered to be undergoing PLM degeneration if five or more of bead or bubble-like structures were observed. For amphid sensory neurons, an animal was considered to be undergoing dendrite degeneration if five or more bead/bubble-like structures were observed, or if one or more vacuoles that have a larger diameter than the dendrites were observed along dendrites. For each time point, independent experiments were performed three times, each consisting of at least 50 live animals. The percentage was calculated by dividing the number of animals having dendrite degeneration by the total number of animals observed. The error bar indicates ± SEM among the three experiments at each time point. Also, a small number (≈15 animals) of control animals were always observed in parallel to non-control animals in each subsequent dendrite degeneration experiment, to ensure the experimental conditions were appropriate and that the % control animals having dendrite degeneration deviated less than 5% from the mean number (for each day) in Fig. 1C. Quantification of dendrite degeneration in *C. elegans* was performed without applying any anesthetics.

For degenerative morphological changes in rat cortical neurons, Sholl analysis was performed using a plug-in for Fiji as described previously (Ferreira et al., 2014).

Quantification of dendrite degeneration was also performed double blind.

Adult Epidermal or PVD-specific RNAi—To knock down gene expression in the adult epidermis or PVD, we expressed *sid-1*(cDNA) under the control of *Pdpy-7*(epidermis) or *Pser-2*(PVD) in an *sid-1 (pk3321)* mutant background. *sid-1* mutants are resistant to RNAi,

and transgenic animals are resistant to RNAi in all tissues except in the cells expressing *sid-1* cDNA. At the L4 stage, we transferred transgene animals to RNAi plates (with FUDR) with bacteria expressing the appropriate double-stranded RNA (dsRNA), and we quantified the degeneration of PVD neurons on each day until Day 9. The RNAi clones were obtained from the Ahringer library and confirmed by sequencing or made by PCR from cDNA. Bacteria expressing empty L4440 plasmid were used as control.

Protein Analysis—For protein expression studies in *C. elegans*, we used an integrated transgene (*yadIs58*) expressing NLP-29::GFP::2A::mCherry driven by its own promoter with its own 3′UTR (pNP140). Synchronous animals were grown on NGM plates with 5′-flurodeoxyuridine (FUDR), and animals were collected at days 1, 3, 5 and 7. Protein was extracted in SDS sample buffer containing 1mM DTT by freeze-thawing for 20–50 cycles between dry ice/ethanol and a 37°C water bath, and then denatured by heating to 95°C for 5 minutes. Bl ots were probed with a rabbit anti-GFP antibody (Sigma, G1544), or a mouse anti-tubulin monoclonal antibody (Life Technologies, 322600), and visualized with Amersham HRP-conjugated anti-rabbit or anti-mouse secondary antibodies at a 1:5000 dilution (GE Healthcare Life Sciences) using the SuperSignal West Femto kit (Pierce, Rockford, IL).

Real-time Reverse Transcription PCR—To measure the change in *nlp-29* mRNA levels during aging, total RNA was isolated from wild-type N2 animals at ages of Day 1, Day 3, Day 5 and Day 7. Animals were washed with M9 buffer three times for 90 minutes in total, and RNA was isolated using TRI Reagent® (Invitrogen). Collection of animals was repeated three independent times for each time point. Reverse transcription was performed on total RNA (1 μg) using an iScript™ Reverse Transcription Supermix for RT-qPCR (Bio-Rad Laboratories). Quantitative real-time, reverse-transcription PCR (qPCR) was performed using iTaq™ Universal Probes Supermix (Bio-Rad Laboratories) and ready-to-use TaqMan Gene Expression Assays (Invitrogen) to quantify the mRNA levels of *nlp-29*, *npr-12*, *act-2*, *ama-1* and *cdc-42*. *act-2*/actin, *ama-1*/RNA polymerase II and *cdc-42*/cell division control protein 42 served as internal controls. qPCR amplifications were performed using an Applied Biosystems StepOnePlus Real-Time PCR System (Applied Biosystems). Relative mRNA levels were quantified using StepOnePlus Software v2.1 based on the *comparative* $\Delta\Delta CT$ method.

Peptide Microinjection—We chemically synthesized the predicted mature NLP-29 peptide of 51 amino acids: QWGYGGYGRGYGGYGGYGRGMYGGYGRGMYGGYGRGMYGGYGRGMYGGWGK (Thermo Scientific); the same was conducted for the NLP-31 peptide of 53 amino acids:

QWGYGGYGRGYGGYGGYGRGYGGYGGYGRGYGGYGRGMYGGYGRPYGGYGWGK. 1 mg of peptide was initially dissolved in 100% DMSO to make a stock concentration of 5 mM. The stock was diluted using a 50% v/v solution of DMSO in M9 buffer, to make a final concentration of 10 μM or 100 μM for injection. The 50% DMSO was used as a vehicle solution for the control group. The peptide was injected from the dorsal side, aimed slightly anterior to the PVD cell body to ensure that the cell body was not disturbed. 24 hours post

injection, PVD dendrite morphology was examined. For each group, at least 50 animals were injected with either the peptide or vehicle.

Live-cell Immunohistochemistry Staining—Live-cell staining was performed as previously described (Saito et al., 2004), to visually confirm the expression and localization of FLAG-NPR-12 and FLAG-NPR-32 on the plasma membrane of HEK293T cells. The anti-FLAG antibody was purchased from Sigma (#F3165) and Alexa Fluor®594-conjugated secondary antibody was purchased from Thermo Fisher Scientific (#A11005).

Live-cell Calcium Imaging—24 hours post transfection, cells were imaged consecutively in three-second intervals using a Zeiss AxioObserver 1.0 inverted microscope. Cells were continuously perfused with bath solution (Hank's buffer containing 10 mM HEPES and 5 mM glucose) using a peristaltic pump, except for the one-minute stimulus period when 10 μM NLP-29 peptide, 10 μM NLP-31 peptide, 16.7 % DMSO (the same concentration of DMSO as in the 10 μM peptide solution), or 1 μM isoproterenol solution was applied manually to the recording chamber. The stimuli were diluted using the perfusion buffer. For each dish, all clear single cells were selected as regions of interest, ranging between 95 to 145 cells in each field. Changes in calcium-dependent fluorescence intensity were quantified by calculating the $\Delta F/F_0$ ratios during the first 120 sec post-stimulus. F_0 corresponds to the first frame after stimulus, whereas ΔF correspond to the difference in fluorescence intensity between F_0 and each individual frame during the first 120 sec post-stimulus. The magnitude of the calcium response was also quantified by integrating the area under the response curve during the first 120 sec post-stimulus. All data analysis was done with MetaFluor, Microsoft Excel, and Graphpad Prism.

Mortality Assay—All mortality assays were performed at 20 °C on NGM plates with FUDR. An experimental pool of at least 50 animals was used for each genotype. Dead animals were counted daily until no animals survived. Lost animals were subtracted from the total number. The experiment was repeated three independent times.

***Pnlp-29::GFP* Scoring—**To quantify *frIs7*(*Pnlp-29::GFP; Pcol-12::dsRed*) induction during aging, hermaphrodites of L4 stage were picked and grown on NGM plates with FUDR to inhibit progeny growth. Each animal was scored as uninduced (red or orange) or induced (yellow, yellow-green, and green) at each time point to estimate the percentage induction in a population. The percentage was calculated by dividing the number of animals with *Pnlp-29::GFP* induction by the total number of animals observed. Three independent experiments were performed, and a total of at least 100 animals were analyzed for each time point. The *Pcol-12* promoter was used to drive epidermis-specific expression of dsRed.

***Drechmeria Coniospora* Infection—**Infection was performed as previously described (Pujol et al., 2008a). Briefly, *D. coniospora* was freshly harvested in 50 mM NaCl to make a solution, and 150 μl of this solution was added to NGM plates (with regular OP50 and without FUDR) containing animals to be infected. Adult worms were infected on either Day 1 or on Day 3. After 36-hour incubation in the pathogen at 20 °C, the animals were used for the quantification of dendrite degeneration. No animals died during the 36-hour infection period. For the control (non-infected) group, a 50 mM NaCl solution of the same volume

was used instead. The infection efficiency was confirmed by scoring *Pnlp-29::GFP* induction in *frIs7* animals that were also treated with *D. coniospora* in parallel to each infection experiment. On average, 90% of the animals had *Pnlp-29::GFP* induction after 36 hours of treatment (Fig. S6A). Dead *D. coniospora* was prepared by heating at 100°C for 60 min.

Hoechst Staining—Worms were washed off plates with M9 buffer, and then incubated in M9 buffer containing 1 μg/mL Hoechst 33258 (Sigma) at room temperature for 15 minutes with gentle agitation, followed by three washes with M9 buffer (Moribe et al., 2004).

PVD Function Analysis - Harsh Touch Response—PVD is responsible for *C. elegans* to respond to harsh touch applied to the mid-part of the body, by initiating forward or backward movements (Chatzigeorgiou et al., 2010; Li et al., 2011; Way and Chalfie, 1989). Activating the touch receptor neurons, including ALM, AVM, PLM and PVM, by gentle touch can also generate similar behavioral responses (Way and Chalfie, 1989). To exclude the possible effects from the touch receptor neurons on our behavioral tests, we assessed PVD function in a *mec-4* mutant background, which lacks functioning touch receptor neurons but has normally-functioning PVD neurons (Driscoll and Chalfie, 1991) (Liu and Shen, 2012). We used *mec-3* mutants, which lack normal functions in both PVD and the touch receptor neurons, as a positive control for the ‘no harsh touch response’ (Liu and Shen, 2012; Way and Chalfie, 1989). The response to harsh touch was measured as previously described (Chalfie and Sulston, 1981; Way and Chalfie, 1989) using a worm pick to poke the midsection of the animal body to estimate the function of PVD neurons. The percentage was calculated by dividing the number of animals NOT responding to the stimuli by the total number of animals examined. Three independent experiments were performed, and a total of at least 100 animals were analyzed for each time point.

Quantification and Statistical Analysis

Data Analysis—For degenerative morphological changes in rat cortical neurons, Sholl analysis was performed using a plug-in for Fiji as described previously (Ferreira et al., 2014).

Statistical Analysis—Data were analyzed using Student’s *t* test, One-way ANOVA followed by Fisher’s LSD post-hoc test, ANCOVA or Fisher’s exact test in GraphPad Prism 6. A *p* value cut-off of 0.05 was considered statistically significant. For aging-associated and infection-associated dendrite degeneration experiments, mortality assays, aging-associated PVD function assays, aging-associated mRNA expression assays, and aging-associated as well as infection-associated *Pnlp-29::GFP* induction assays, the means shown in the figures indicate the mean values calculated from at least three technical replicates, and at least 50 animals were included for quantification in each technical replicate. The error bars in the figures indicate ± SEM.

Supplementary Material

Refer to Web version on PubMed Central for supplementary material.

Acknowledgments

We thank Dr. Yuji Kohara for providing cDNAs used in this study. Some strains used in this study were provided by National BioResource Project (NBRP, Japan), as well as the Caenorhabditis Genetics Center (CGC), which is funded by the NIH Office of Research Infrastructure Programs (P40 OD010440). We thank Dr. Yishi Jin, Dr. Jonathan Ewbank, Dr. Kang Shen and our lab members for comments on the manuscript. We thank Oluwadamilola Lawal for culturing rat cortical neurons. We thank Shizue Omi-Massieau for culturing and preparing *D. coniospora* plates. N.P. is supported by CNRS and ANR [ANR-12-BSV3-0001-01, ANR-11-LABX-0054 (Labex INFORM) and ANR-16-CE15-0001-01]. M.C. was supported by the UCSD Cellular and Molecular Genetics Training Grant (NIH T32 GM007240) and by NIH R01 (GM054657 to A.D.C). T.Z., R.S and H.M. are supported by NIH R01 (DC014423 to H.M.). This project is supported by NIH R00 (NS076646 to D.Y.) and Holland-Trice scholars award, and L.E and D.Y. are also supported by NIH R01 (NS094171 to D.Y.).

References

Adalbert R, Coleman MP. Review: Axon pathology in age-related neurodegenerative disorders. Neuropathol Appl Neurobiol. 2013; 39:90–108. [PubMed: 23046254]

Albeg A, Smith CJ, Chatzigeorgiou M, Feitelson DG, Hall DH, Schafer WR, Miller DM 3rd, Treinin M. *C. elegans* multi-dendritic sensory neurons: morphology and function. Mol Cell Neurosci. 2011; 46:308–317. [PubMed: 20971193]

Apfeld J, Kenyon C. Cell nonautonomy of *C. elegans daf-2* function in the regulation of diapause and life span. Cell. 1998; 95:199–210. [PubMed: 9790527]

Boulanger LM. Immune proteins in brain development and synaptic plasticity. Neuron. 2009; 64:93–109. [PubMed: 19840552]

Brenner S. The genetics of *Caenorhabditis elegans*. Genetics. 1974; 77:71–94. [PubMed: 4366476]

Chalfie M, Sulston J. Developmental genetics of the mechanosensory neurons of *Caenorhabditis elegans*. Dev Biol. 1981; 82:358–370. [PubMed: 7227647]

Chatzigeorgiou M, Yoo S, Watson JD, Lee WH, Spencer WC, Kindt KS, Hwang SW, Miller DM 3rd, Treinin M, Driscoll M, Schafer WR. Specific roles for DEG/ENaC and TRP channels in touch and thermosensation in *C. elegans* nociceptors. Nat Neurosci. 2010; 13:861–868. [PubMed: 20512132]

Chu H, Mazmanian SK. Innate immune recognition of the microbiota promotes host-microbial symbiosis. Nat Immunol. 2013; 14:668–675. [PubMed: 23778794]

Clark SG, Chiu C. *C. elegans* ZAG-1, a Zn-finger-homeodomain protein, regulates axonal development and neuronal differentiation. Development. 2003; 130:3781–3794. [PubMed: 12835394]

Couillault C, Pujol N, Reboul J, Sabatier L, Guichou JF, Kohara Y, Ewbank JJ. TLR-independent control of innate immunity in Caenorhabditis elegans by the TIR domain adaptor protein TIR-1, an ortholog of human SARM. Nat Immunol. 2004; 5:488–494. [PubMed: 15048112]

Dickstein DL, Kabaso D, Rocher AB, Luebke JI, Wearne SL, Hof PR. Changes in the structural complexity of the aged brain. Aging Cell. 2007; 6:275–284. [PubMed: 17465981]

Dierking K, Polanowska J, Omi S, Engelmann I, Gut M, Lembo F, Ewbank JJ, Pujol N. Unusual regulation of a STAT protein by an SLC6 family transporter in *C. elegans* epidermal innate immunity. Cell Host Microbe. 2011; 9:425–435. [PubMed: 21575913]

Dong X, Liu OW, Howell AS, Shen K. An extracellular adhesion molecule complex patterns dendritic branching and morphogenesis. Cell. 2013; 155:296–307. [PubMed: 24120131]

Driscoll M, Chalfie M. The *mec-4* gene is a member of a family of *Caenorhabditis elegans* genes that can mutate to induce neuronal degeneration. Nature. 1991; 349:588–593. [PubMed: 1672038]

Feng T, Tammineni P, Agrawal C, Jeong YY, Cai Q. Autophagy-mediated Regulation of BACE1 Protein Trafficking and Degradation. J Biol Chem. 2017; 292:1679–1690. [PubMed: 28028177]

Ferreira TA, Blackman AV, Oyrer J, Jayabal S, Chung AJ, Watt AJ, Sjostrom PJ, van Meyel DJ. Neuronal morphometry directly from bitmap images. Nat Methods. 2014; 11:982–984. [PubMed: 25264773]

Frooninckx L, Van Rompay L, Temmerman L, Van Sinay E, Beets I, Janssen T, Husson SJ, Schoofs L. Neuropeptide GPCRs in *C. elegans*. Front Endocrinol (Lausanne). 2012; 3:167. [PubMed: 23267347]

Garden GA, La Spada AR. Intercellular (mis)communication in neurodegenerative disease. Neuron. 2012; 73:886–901. [PubMed: 22405200]

Garigan D, Hsu AL, Fraser AG, Kamath RS, Ahringer J, Kenyon C. Genetic analysis of tissue aging in *Caenorhabditis elegans*: a role for heat-shock factor and bacterial proliferation. Genetics. 2002; 161:1101–1112. [PubMed: 12136014]

Greenwood SM, Mizielinska SM, Frenguelli BG, Harvey J, Connolly CN. Mitochondrial dysfunction and dendritic beading during neuronal toxicity. J Biol Chem. 2007; 282:26235–26244. [PubMed: 17616519]

Herndon LA, Schmeissner PJ, Dudaronek JM, Brown PA, Listner KM, Sakano Y, Paupard MC, Hall DH, Driscoll M. Stochastic and genetic factors influence tissue-specific decline in ageing *C. elegans*. Nature. 2002; 419:808–814. [PubMed: 12397350]

Hickman SE, Kingery ND, Ohsumi TK, Borowsky ML, Wang LC, Means TK, El Khoury J. The microglial sensome revealed by direct RNA sequencing. Nat Neurosci. 2013; 16:1896–1905. [PubMed: 24162652]

Hill JM, Clement C, Pogue AI, Bhattacharjee S, Zhao Y, Lukiw WJ. Pathogenic microbes, the microbiome, and Alzheimer's disease (AD). Front Aging Neurosci. 2014; 6:127. [PubMed: 24982633]

Ilieva H, Polymenidou M, Cleveland DW. Non-cell autonomous toxicity in neurodegenerative disorders: ALS and beyond. J Cell Biol. 2009; 187:761–772. [PubMed: 19951898]

Jack CR Jr, Knopman DS, Jagust WJ, Petersen RC, Weiner MW, Aisen PS, Shaw LM, Vemuri P, Wiste HJ, Weigand SD, et al. Tracking pathophysiological processes in Alzheimer's disease: an updated hypothetical model of dynamic biomarkers. Lancet Neurol. 2013; 12:207–216. [PubMed: 23332364]

Kaul M, Zheng J, Okamoto S, Gendelman HE, Lipton SA. HIV-1 infection and AIDS: consequences for the central nervous system. Cell Death Differ. 2005; 12(Suppl 1):878–892. [PubMed: 15832177]

Kuchibhotla KV, Goldman ST, Lattarulo CR, Wu HY, Hyman BT, Bacskai BJ. Abeta plaques lead to aberrant regulation of calcium homeostasis in vivo resulting in structural and functional disruption of neuronal networks. Neuron. 2008; 59:214–225. [PubMed: 18667150]

Kumar DK, Choi SH, Washicosky KJ, Eimer WA, Tucker S, Ghofrani J, Lefkowitz A, McColl G, Goldstein LE, Tanzi RE, Moir RD. Amyloid-beta peptide protects against microbial infection in mouse and worm models of Alzheimer's disease. Sci Transl Med. 2016; 8:340ra372.

Labed SA, Omi S, Gut M, Ewbank JJ, Pujol N. The pseudokinase NIPI-4 is a novel regulator of antimicrobial peptide gene expression. PLoS One. 2012; 7:e33887. [PubMed: 22470487]

Lesne SE, Sherman MA, Grant M, Kuskowski M, Schneider JA, Bennett DA, Ashe KH. Brain amyloid-beta oligomers in ageing and Alzheimer's disease. Brain. 2013; 136:1383–1398. [PubMed: 23576130]

Li W, Kang L, Piggott BJ, Feng Z, Xu XZ. The neural circuits and sensory channels mediating harsh touch sensation in *Caenorhabditis elegans*. Nat Commun. 2011; 2:315. [PubMed: 21587232]

Lin YC, Koleske AJ. Mechanisms of synapse and dendrite maintenance and their disruption in psychiatric and neurodegenerative disorders. Annu Rev Neurosci. 2010; 33:349–378. [PubMed: 20367247]

Liu OW, Shen K. The transmembrane LRR protein DMA-1 promotes dendrite branching and growth in *C. elegans*. Nat Neurosci. 2012; 15:57–63.

Lu Q, Yang P, Huang X, Hu W, Guo B, Wu F, Lin L, Kovacs AL, Yu L, Zhang H. The WD40 repeat PtdIns(3)P-binding protein EPG-6 regulates progression of omegasomes to autophagosomes. Dev Cell. 2011; 21:343–357. [PubMed: 21802374]

Luallen RJ, Troemel ER. Breaking barriers: a GPCR triggers immunity in nematodes. Nat Immunol. 2014; 15:826–828. [PubMed: 25137464]

Manil-Segalen M, Lefebvre C, Jenzer C, Trichet M, Boulogne C, Satiat-Jeunemaitre B, Legouis R. The C. elegans LC3 acts downstream of GABARAP to degrade autophagosomes by interacting with the HOPS subunit VPS39. Dev Cell. 2014; 28:43–55. [PubMed: 24374177]

Mello CC, Kramer JM, Stinchcomb D, Ambros V. Efficient gene transfer in *C.elegans*: extrachromosomal maintenance and integration of transforming sequences. EMBO J. 1991; 10:3959–3970. [PubMed: 1935914]

Menzies FM, Fleming A, Rubinsztein DC. Compromised autophagy and neurodegenerative diseases. Nat Rev Neurosci. 2015; 16:345–357. [PubMed: 25991442]

Moribe H, Yochem J, Yamada H, Tabuse Y, Fujimoto T, Mekada E. Tetraspanin protein (TSP-15) is required for epidermal integrity in *Caenorhabditis elegans*. J Cell Sci. 2004; 117:5209–5220. [PubMed: 15454573]

Morsch M, Radford R, Lee A, Don EK, Badrock AP, Hall TE, Cole NJ, Chung R. In vivo characterization of microglial engulfment of dying neurons in the zebrafish spinal cord. Front Cell Neurosci. 2015; 9:321. [PubMed: 26379496]

Nathoo AN, Moeller RA, Westlund BA, Hart AC. Identification of neuropeptide-like protein gene families in *Caenorhabditis elegans* and other species. Proc Natl Acad Sci U S A. 2001; 98:14000–14005. [PubMed: 11717458]

Offermanns S, Simon MI. G alpha 15 and G alpha 16 couple a wide variety of receptors to phospholipase C. J Biol Chem. 1995; 270:15175–15180. [PubMed: 7797501]

Oren-Suissa M, Hall DH, Treinin M, Shemer G, Podbilewicz B. The fusogen EFF-1 controls sculpting of mechanosensory dendrites. Science. 2010; 328:1285–1288. [PubMed: 20448153]

Pan CL, Peng CY, Chen CH, McIntire S. Genetic analysis of age-dependent defects of the *Caenorhabditis elegans* touch receptor neurons. Proc Natl Acad Sci U S A. 2011; 108:9274–9279. [PubMed: 21571636]

Pujol N, Cypowyj S, Ziegler K, Millet A, Astrain A, Goncharov A, Jin Y, Chisholm AD, Ewbank JJ. Distinct innate immune responses to infection and wounding in the *C. elegans* epidermis. Curr Biol. 2008a; 18:481–489. [PubMed: 18394898]

Pujol N, Zugasti O, Wong D, Couillault C, Kurz CL, Schulenburg H, Ewbank JJ. Anti-fungal innate immunity in *C. elegans* is enhanced by evolutionary diversification of antimicrobial peptides. PLoS Pathog. 2008b; 4:e1000105. [PubMed: 18636113]

Richardson CE, Spilker KA, Cueva JG, Perrino J, Goodman MB, Shen K. PTRN-1, a microtubule minus end-binding CAMSAP homolog, promotes microtubule function in *Caenorhabditis elegans* neurons. Elife. 2014; 3:e01498. [PubMed: 24569477]

Risher WC, Patel S, Kim IH, Uezu A, Bhagat S, Wilton DK, Pilaz LJ, Singh Alvarado J, Calhan OY, Silver DL, et al. Astrocytes refine cortical connectivity at dendritic spines. Elife. 2014; 3

Saito H, Kubota M, Roberts RW, Chi Q, Matsunami H. RTP family members induce functional expression of mammalian odorant receptors. Cell. 2004; 119:679–691. [PubMed: 15550249]

Salzberg Y, Diaz-Balzac CA, Ramirez-Suarez NJ, Attreed M, Tecle E, Desbois M, Kaprielian Z, Bulow HE. Skin-derived cues control arborization of sensory dendrites in *Caenorhabditis elegans*. Cell. 2013; 155:308–320. [PubMed: 24120132]

Sekar A, Bialas AR, de Rivera H, Davis A, Hammond TR, Kamitaki N, Tooley K, Presumey J, Baum M, Van Doren V, et al. Schizophrenia risk from complex variation of complement component 4. Nature. 2016; 530:177–183. [PubMed: 26814963]

Shao Z, Watanabe S, Christensen R, Jorgensen EM, Colon-Ramos DA. Synapse location during growth depends on glia location. Cell. 2013; 154:337–350. [PubMed: 23870123]

Smith CJ, Watson JD, Spencer WC, O'Brien T, Cha B, Albeg A, Treinin M, Miller DM 3rd. Time-lapse imaging and cell-specific expression profiling reveal dynamic branching and molecular determinants of a multi-dendritic nociceptor in *C. elegans*. Dev Biol. 2010; 345:18–33. [PubMed: 20537990]

Stawicki TM, Zhou K, Yochem J, Chen L, Jin Y. TRPM channels modulate epileptic-like convulsions via systemic ion homeostasis. Curr Biol. 2011; 21:883–888. [PubMed: 21549603]

Stephan AH, Barres BA, Stevens B. The complement system: an unexpected role in synaptic pruning during development and disease. Annu Rev Neurosci. 2012; 35:369–389. [PubMed: 22715882]

Stephan AH, Madison DV, Mateos JM, Fraser DA, Lovelett EA, Coutellier L, Kim L, Tsai HH, Huang EJ, Rowitch DH, et al. A dramatic increase of C1q protein in the CNS during normal aging. J Neurosci. 2013; 33:13460–13474. [PubMed: 23946404]

Su JH, Cummings BJ, Cotman CW. Identification and distribution of axonal dystrophic neurites in Alzheimer's disease. Brain Res. 1993; 625:228–237. [PubMed: 8275305]

Tao J, Rolls MM. Dendrites have a rapid program of injury-induced degeneration that is molecularly distinct from developmental pruning. J Neurosci. 2011; 31:5398–5405. [PubMed: 21471375]

Veriepe J, Fossouo L, Parker JA. Neurodegeneration in *C. elegans* models of ALS requires TIR-1/Sarm1 immune pathway activation in neurons. Nat Commun. 2015; 6:7319. [PubMed: 26059317]

Wang JT, Medress ZA, Barres BA. Axon degeneration: molecular mechanisms of a self-destruction pathway. J Cell Biol. 2012; 196:7–18. [PubMed: 22232700]

Wang Y, Mandelkow E. Tau in physiology and pathology. Nat Rev Neurosci. 2016; 17:5–21. [PubMed: 26631930]

Way JC, Chalfie M. The *mec-3* gene of *Caenorhabditis elegans* requires its own product for maintained expression and is expressed in three neuronal cell types. Genes Dev. 1989; 3:1823–1833. [PubMed: 2576011]

White JG, Southgate E, Thomson JN, Brenner S. The structure of the ventral nerve cord of *Caenorhabditis elegans*. Philos Trans R Soc Lond B Biol Sci. 1976; 275:327–348. [PubMed: 8806]

White JG, Southgate E, Thomson JN, Brenner S. The structure of the nervous system of the nematode *Caenorhabditis elegans*. Philos Trans R Soc Lond B Biol Sci. 1986; 314:1–340. [PubMed: 22462104]

Williams WM, Torres S, Siedlak SL, Castellani RJ, Perry G, Smith MA, Zhu X. Antimicrobial peptide beta-defensin-1 expression is upregulated in Alzheimer's brain. J Neuroinflammation. 2013; 10:127. [PubMed: 24139179]

Wu F, Li Y, Wang F, Noda NN, Zhang H. Differential function of the two Atg4 homologues in the aggrephagy pathway in *Caenorhabditis elegans*. J Biol Chem. 2012; 287:29457–29467. [PubMed: 22767594]

Yu WH, Cuervo AM, Kumar A, Peterhoff CM, Schmidt SD, Lee JH, Mohan PS, Mercken M, Farmery MR, Tjernberg LO, et al. Macroautophagy–a novel Beta-amyloid peptide-generating pathway activated in Alzheimer's disease. J Cell Biol. 2005; 171:87–98. [PubMed: 16203860]

Zhang H, Chang JT, Guo B, Hansen M, Jia K, Kovacs AL, Kumsta C, Lapierre LR, Legouis R, Lin L, et al. Guidelines for monitoring autophagy in Caenorhabditis elegans. Autophagy. 2015; 11:9–27. [PubMed: 25569839]

Zhang LJ, Gallo RL. Antimicrobial peptides. Curr Biol. 2016; 26:R14–R19. [PubMed: 26766224]

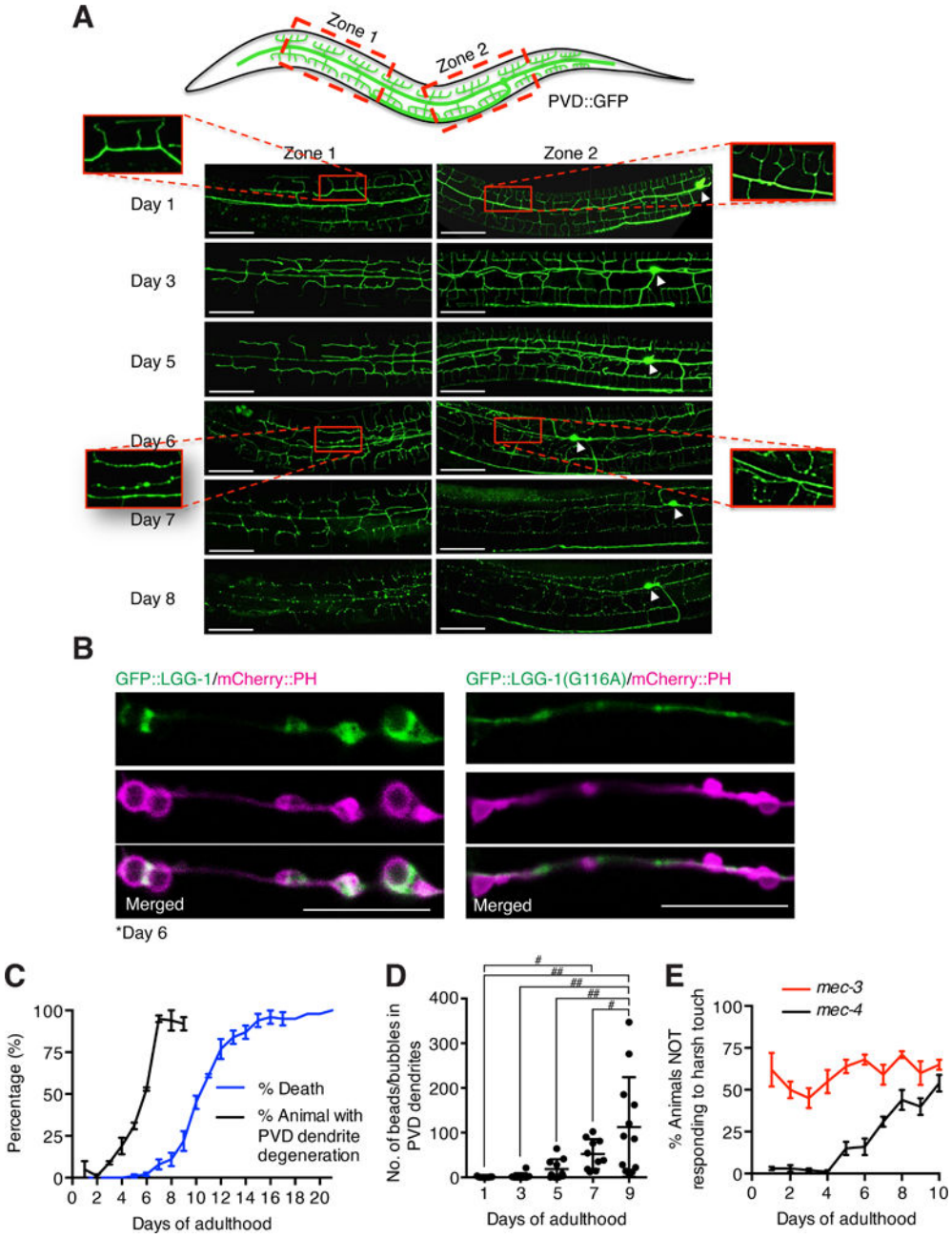

Figure 1. Characterization of aging-associated PVD dendrite degeneration

(A) Representative images of PVD dendrite degeneration in control animals (*wdIs51*) during aging. White arrows: PVD cell bodies. Scale bars: 50 μm.

(B) Representative images of co-localization of autophagosomes (GFP::LGG-1) and dendrite degeneration-associated bead or bubble-like structures (mCherry::PH/membrane-bound mCherry) in the PVD neuron of control animals. A mutant form of LGG-1 (G116A) that does not have the ability to localize to autophagosomes was used as a negative control (Manil-Segalen et al., 2014). Scale bars: 10 μm.

(C) Quantification of PVD dendrite degeneration and the mortality (death) rate in control animals (*wdIs51*). For each experiment, the percentage was calculated by the number of

animals having dendrite degeneration divided by the total number of animals observed. The error bar indicates ± SEM among the three experiments performed for each time point.
(D) The severity of PVD dendrite degeneration in control animals. Each dot represents an individual animal. $n = 10\sim12$. One-way ANOVA, followed by Fisher's LSD post-hoc test. # $p < 0.05$, ## $p < 0.001$.
(E) PVD function analysis in *mec-4* mutants as the reference strain, and in *mec-3* mutants as a positive control for NOT responding to harsh touch.
Data are represented as mean ± SEM.
See also Figure S1 and Figure S2.

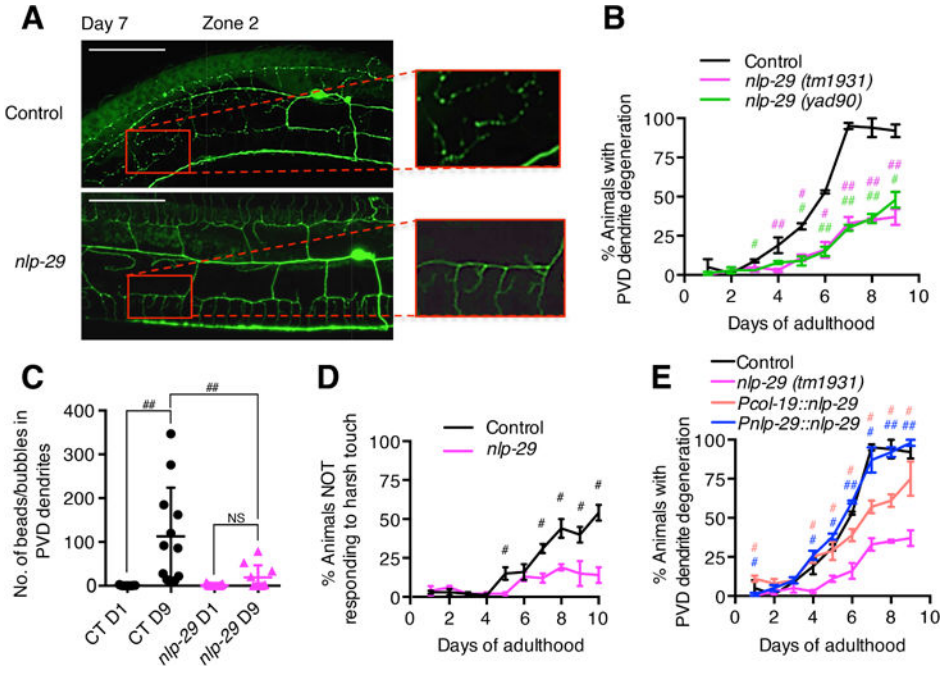

Figure 2. Loss-of-function mutation of *nlp-29*/AMP delays the onset of aging-associated PVD dendrite degeneration

(A) Representative images of PVD neurons in control animals (*wdIs51*) and *nlp-29* (*tm1931*) mutants on Day 7. Zone 2 is same as illustrated in Figure 1A. Scale bars: 50 μm. *The weak GFP signal in the intestine is gut auto-fluorescence, which is commonly observed in aged animals.

(B) PVD dendrite degeneration in loss-of-function of *nlp-29(tm1931)* and *nlp-29(yad90)*. Student's *t*-test for each day. *nlp-29(tm1931)* versus control: #(pink) $p < 0.05$, ##(pink) $p < 0.001$; *nlp-29(yad90)* versus control: #(green) $p < 0.05$, ##(green) $p < 0.001$.

(C) The severity of PVD dendrite degeneration in control and *nlp-29(tm1931)* animals on Day 1 and Day 9. Each dot represents an individual animal. $n = 10$~12. One-way ANOVA, followed by Fisher's LSD post-hoc test. ## $p < 0.001$. CT, control; NS, not significant.

(D) PVD function analysis in *mec-4* (labeled as control) and *nlp-29(tm1931);mec-4* (labeled as *nlp-29*). Student's *t*-test, #$p < 0.05$ for *nlp-29* versus control animals for each day.

(E) PVD dendrite degeneration in *nlp-29(tm1931)* and rescue transgenic strains. Epidermis-specific rescue was performed using the *col-19* promoter. Student's *t*-test was used to determine the difference between *nlp-29(tm1931)* and each rescue strain, for each day. *Pcol-19::nlp-29* rescue versus *nlp-29(tm1931)*: #(orange)$p < 0.05$; *Pnlp-29::nlp-29* rescue versus *nlp-29(tm1931)*: #(blue)$p < 0.05$, ##(blue)$p < 0.001$.

Data are represented as mean ± SEM. Non-significant comparisons are not indicated in the figure.

See also Figure S1, Figure S2, Figure S3 and Figure S4.

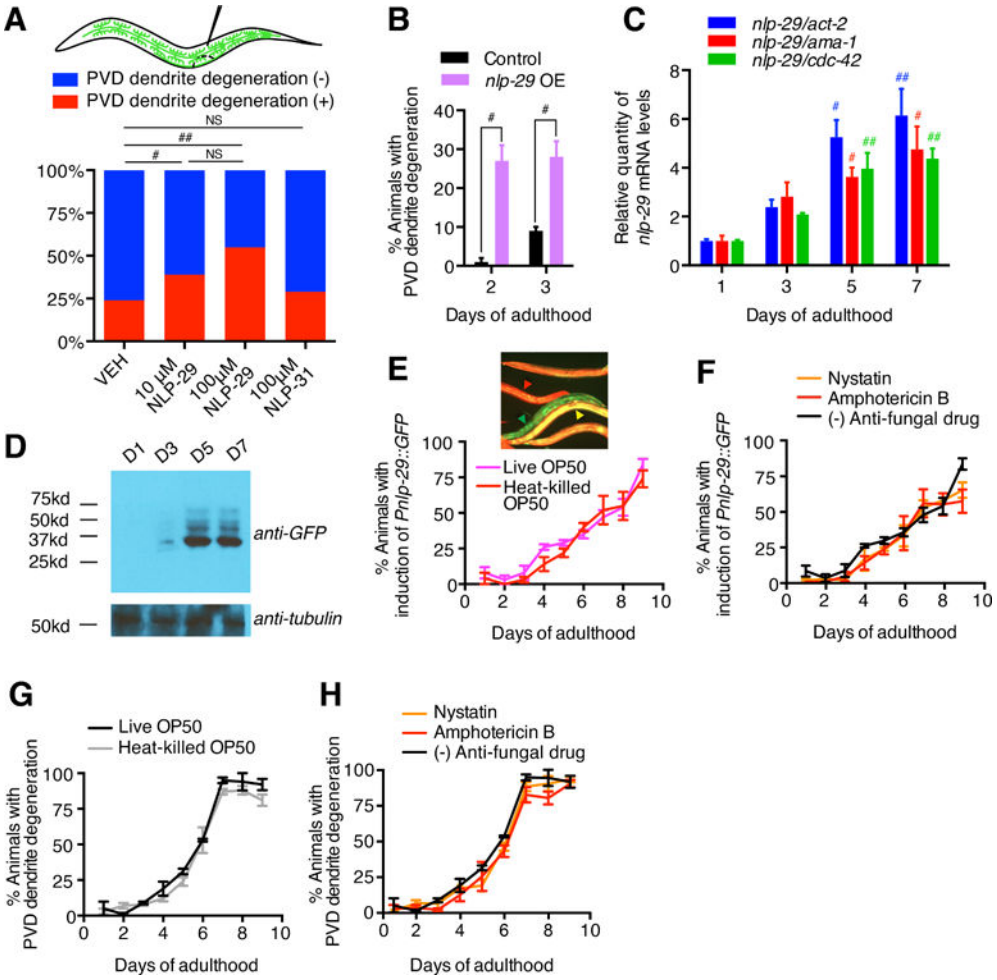

Figure 3. NLP-29/AMP non-cell autonomously triggers aging-associated PVD dendrite degeneration

(A) Microinjection of synthetic NLP-29 peptide and NLP-31 peptide into control animals (*wdIs51*). Injection was performed at age of Day 1, and the PVD dendrite degeneration phenotype was examined 24 hours post injection. Fisher's exact test, #$p < 0.05$, ##$p < 0.001$. VEH, vehicle, 50 % v/v DMSO in M9 buffer. VEH: $n = 146$; 10 μm NLP-29: $n = 66$; 100 μm NLP-29: $n = 64$; 100 μm NLP-31: $n = 68$; where n indicates the number of animals.

(B) Quantification of PVD dendrite degeneration induced by epidermal *nlp-29* overexpression (OE), driven by the *col-19* promoter, in young control animals. Student's *t*-test, #$p < 0.05$.

(C) Age-dependent changes of *nlp-29* mRNA level in control animals. *act-2*, *ama-1* and *cdc-42* were used as reference genes. Mean differences between different age groups were analyzed by one-way ANOVA for each reference gene, followed by Fisher's LSD post-hoc test. # $p < 0.05$, ## $p < 0.001$ for versus Day 1.

(D) Western blot results of *Pnlp-29::NLP-29::GFP* expression in control animals over the course of aging. See two more repeats in Figure S3D.

(E) Age-dependent changes of *Pnlp-29::GFP* induction in control animals [*frIs7 (Pnlp-29::GFP; Pcol-12::dsRed)*] grown on live OP50 or heat-killed OP50. *Pcol-12* is an

epidermis-specific promoter. A representative image of *frIs7* under 10X magnification is shown. Red arrow: an animal without *Pnlp-29::GFP* induction (appears red or orange); yellow and green arrow: animals with *Pnlp-29::GFP* induction (appear yellow, yellow-green, or green). Student's *t* test showed no differences between the live OP50 condition and heat-killed OP50 condition at any time point.

(F) Age-dependent changes of *Pnlp-29::GFP* induction in control animals (*frIs7)* grown on NGM plates supplemented with anti-fungal drugs (either 10 μg/mL nystatin or amphotericin B 1.6 μg/mL). Student's *t* test showed no differences between drug (−) condition and each drug (+) condition at any time point.

(G) PVD dendrite degeneration rate of control animals (*wdIs51*) grown on live OP50 or heat-killed OP50. Student's *t* test showed no differences between the two conditions at any time point.

(H) PVD dendrite degeneration rate of control animals (*wdIs51*) grown on NGM plates supplemented with anti-fungal drugs (either 10 μg/mL nystatin or amphotericin B 1.6 μg/mL). Student's *t* test showed no differences between drug (−) condition and each drug (+) condition at any time point.

Data are represented as mean ± SEM. Non-significant comparisons are not indicated in the figure.

See also Figure S3 and Figure S4.

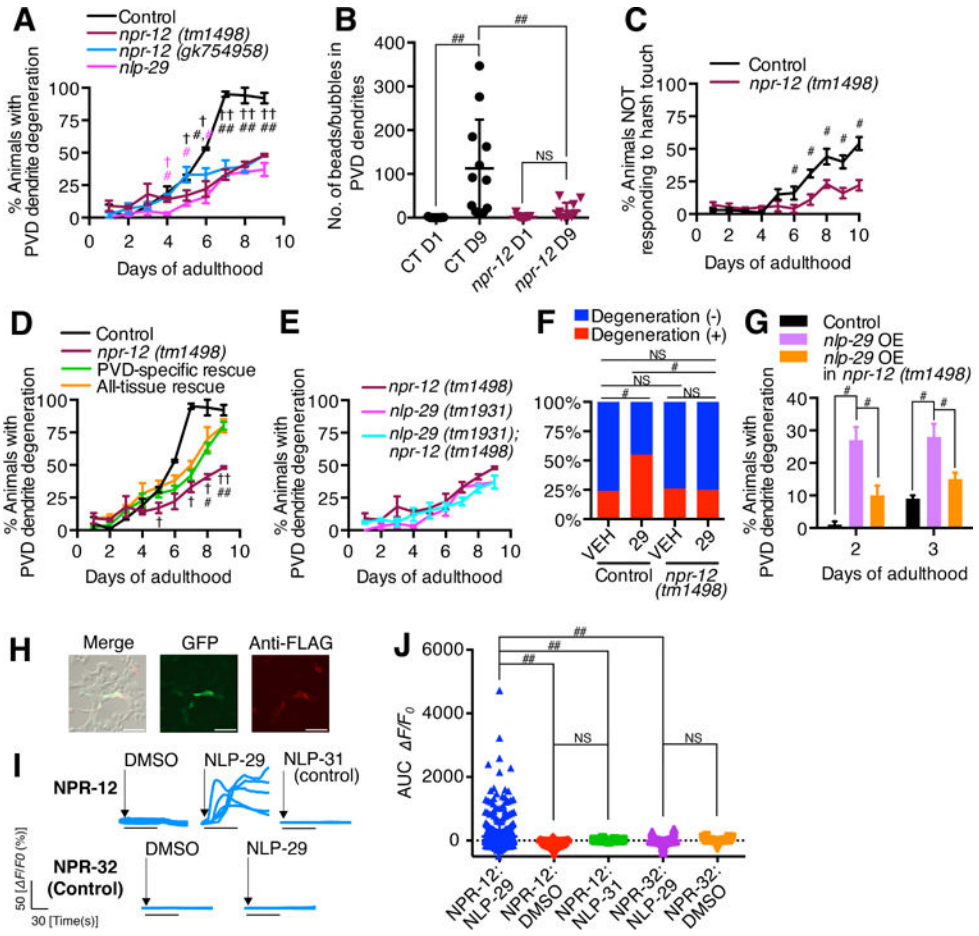

Figure 4. NLP-29 regulates PVD dendrite degeneration through activating NPR-12/neuronal GPCR

(A) PVD dendrite degeneration in *npr-12(tm1498)* and *npr-12(gk754958)* mutants. One-way ANOVA, followed by Fisher's LSD post-hoc test, was used to detect the differences between each *npr-12* strain, control and *nlp-29(tm1931)*, for each day. *npr-12(tm1498)* versus control: †(black) $p < 0.05$, ††(black) $p < 0.001$. *npr-12(tm1498)* versus *nlp-29*: †(pink) $p < 0.05$. *npr-12(gk754958)* versus control: #(black) $p < 0.05$, ##(black) $p < 0.001$. *npr-12(gk754958)* versus *nlp-29*: #(pink) $p < 0.05$.

(B) The severity of PVD dendrite degeneration in control and *npr-12(tm1498)* animals on Day 1 and Day 9. Each dot represents an individual animal. $n = 10$~12. One-way ANOVA, followed by Fisher's LSD post-hoc test. ## $p < 0.001$. CT, control; NS, not significant.

(C) PVD function analysis in *mec-4* (labeled as control) and *npr-12;mec-4* (labeled as *npr-12*). Student's *t* test, # $p < 0.05$ for control versus *npr-12* for each day.

(D) PVD dendrite degeneration in *npr-12(tm1498)*, all-tissue as well as PVD-specific rescue strains. The *dpy-30* promoter and *ser-2(3)* promoter were used to express *npr-12* cDNA in all tissues and PVD, respectively. One-way ANOVA, followed by Fisher's LSD post-hoc, was used to determine the difference between *npr-12* and both rescue strains. PVD-specific rescue versus *npr-12*: # $p < 0.05$, ## $p < 0.001$. All-tissue rescue versus *npr-12*: † $p < 0.05$, †† $p < 0.001$. No differences were detected between all-tissue and PVD-specific rescues strains at any time point.

(E) PVD dendrite degeneration in *nlp-29;npr-12* double mutants. One-way ANOVA showed no differences between *nlp-29;npr-12*, *nlp-29* single mutants, and *npr-12* single mutants at any time point.

(F) PVD dendrite degeneration in control (*wdIs51*) and *npr-12(tm1498)* animals microinjected with 100 μM synthetic NLP-29 peptide. Injection was performed at age of Day 1, and PVD dendrite degeneration was examined 24 hours post injection. Control animals: DMSO group: $n = 146$; NLP-29 group: $n = 64$. *npr-12* mutants: DMSO group: $n = 46$; NLP-29 group: $n = 65$; where n indicates the number of animals. Fisher's exact test, # $p < 0.05$; NS, not significant; VEH, vehicle; 29, NLP-29 peptide.

(G) PVD dendrite degeneration induced by *nlp-29* overexpression (OE) in *npr-12(tm1498)* mutants. The *col-19* promoter was used to drive *nlp-29* OE in the epidermis. One-way ANOVA, followed by Fisher's LSD post-hoc test, was used to detect the differences between groups on each day. # $p < 0.05$.

(H) Live-cell surface staining of HEK293T cells co-transfected with GFP and N-terminal FLAG-tagged NPR-12. Cells were stained with anti-FLAG antibody. Scale bars = 50 μm.

(I) Calcium imaging of HEK293T cells transfected with NPR-12 or NPR-32. Representative calcium responses during the first 120 sec after stimulating with DMSO, 10 μM NLP-29, or 10 μM NLP-31 are shown. The responses were calculated as the change in fluorescence (ΔF) over the initial fluorescence (F_0). The bar beneath the trace indicates the time period when the stimulus was being applied. All traces from all dishes are shown in Figure S6.

(J) The area under the curve (AUC) of $\Delta F/F_0$ intensity was used to show the calcium response of individual cells to each stimulus. $\Delta F/F_0$ intensity within the first 120 sec after stimulus application was included for quantification. Data was analyzed by one-way ANOVA, followed by Fisher's LSD post-hoc test. ## $p < 0.001$, NS, not significant. NPR-12:NLP-29, $n = 593$; NPR-12:DMSO, $n = 396$; NPR-12:NLP-31, $n = 97$; NPR-32:NLP-29, $n = 152$; NPR-32:DMSO, $n = 152$; where n indicates the number of cells. Data are represented as mean ± SEM. Non-significant comparisons are not indicated in the figure.

See also Figure S1, Figure S2, Figure S5 and Figure S6.

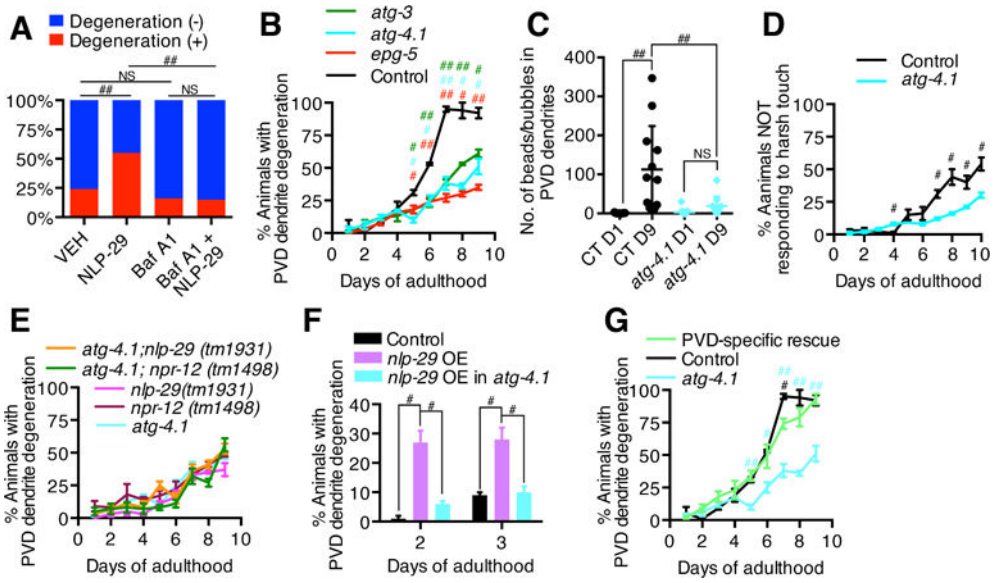

Figure 5. Autophagy machinery acts downstream of NPR-12/neuronal GPCR

(A) PVD dendrite degeneration in control animals (*wdIs51*) microinjected with 100 μM NLP-29 peptide and 50 μM bafilomycin A1 (Baf A1), an autophagy inhibitor. Injection was performed at age of Day 1, and PVD dendrite degeneration phenotype was examined 24 hours post injection. Fisher's exact test, ##$p < 0.001$. VEH, vehicle, 50 % v/v DMSO in M9 buffer; NS, not significant. VEH: $n = 146$; NLP-29: $n = 64$; Baf A1: $n = 123$; Baf A1 + NLP-29: $n = 117$; where n indicates the number of animals.

(B) PVD dendrite degeneration in mutants of autophagy-related genes, *atg-3*, *atg-4.1* and *epg-5*. Student's *t*-test was used to detect the differences between each mutant and control animals. *atg-3* versus control: #(green) $p < 0.05$, ##(green) $p < 0.001$. *atg-4.1* versus control: #(blue) $p < 0.05$, ##(blue) $p < 0.001$. *epg-5* versus control: #(red) $p < 0.05$, ##(red) $p < 0.001$.

(C) The severity of PVD dendrite degeneration in control and *atg-4.1(lf)* animals on Day 1 and Day 9. Each dot represents an individual animal. $n = 10$~12. One-way ANOVA, followed by Fisher's LSD post-hoc test. ## $p < 0.001$. CT, control; NS, not significant.

(D) PVD function analysis in *mec-4* (labeled as control) and *atg-4.1;mec-4* (labeled as *atg-4.1*). Student's *t* test, # $p < 0.05$ for control versus *atg-4.1* for each day.

(E) PVD dendrite degeneration in *atg-4.1;nlp-29(tm1931) and atg-4.1;npr-12(tm1498)*. One-way ANOVA showed no differences between *atg-4.1;npr-12*, *atg-4.1;nlp-29*, *nlp-29* single mutants, and *npr-12* single mutants, at any time point.

(F) PVD dendrite degeneration induced by *nlp-29* overexpression (OE) in control and *atg-4.1* mutants. The *col-19* promoter was used to drive *nlp-29* OE in the epidermis. One-way ANOVA, followed by Fisher's LSD post-hoc test, for each day. # $p < 0.05$.

(G) PVD dendrite degeneration in *atg-4.1* mutants and PVD-specific rescue strain. The *ser-2(3)* promoter was used to express *atg-4.1* cDNA in PVD neurons. One-way ANOVA, followed by Fisher's LSD post-hoc, for each day. PVD-specific rescue versus control: #(black) $p < 0.05$. PVD-specific rescue versus *atg-4.1*: #(blue) $p < 0.05$, ##(blue) $p < 0.001$. Data are represented as mean ± SEM. Non-significant comparisons are not indicated in the figure.

See also Figure S1, Figure S2 and Figure S3.

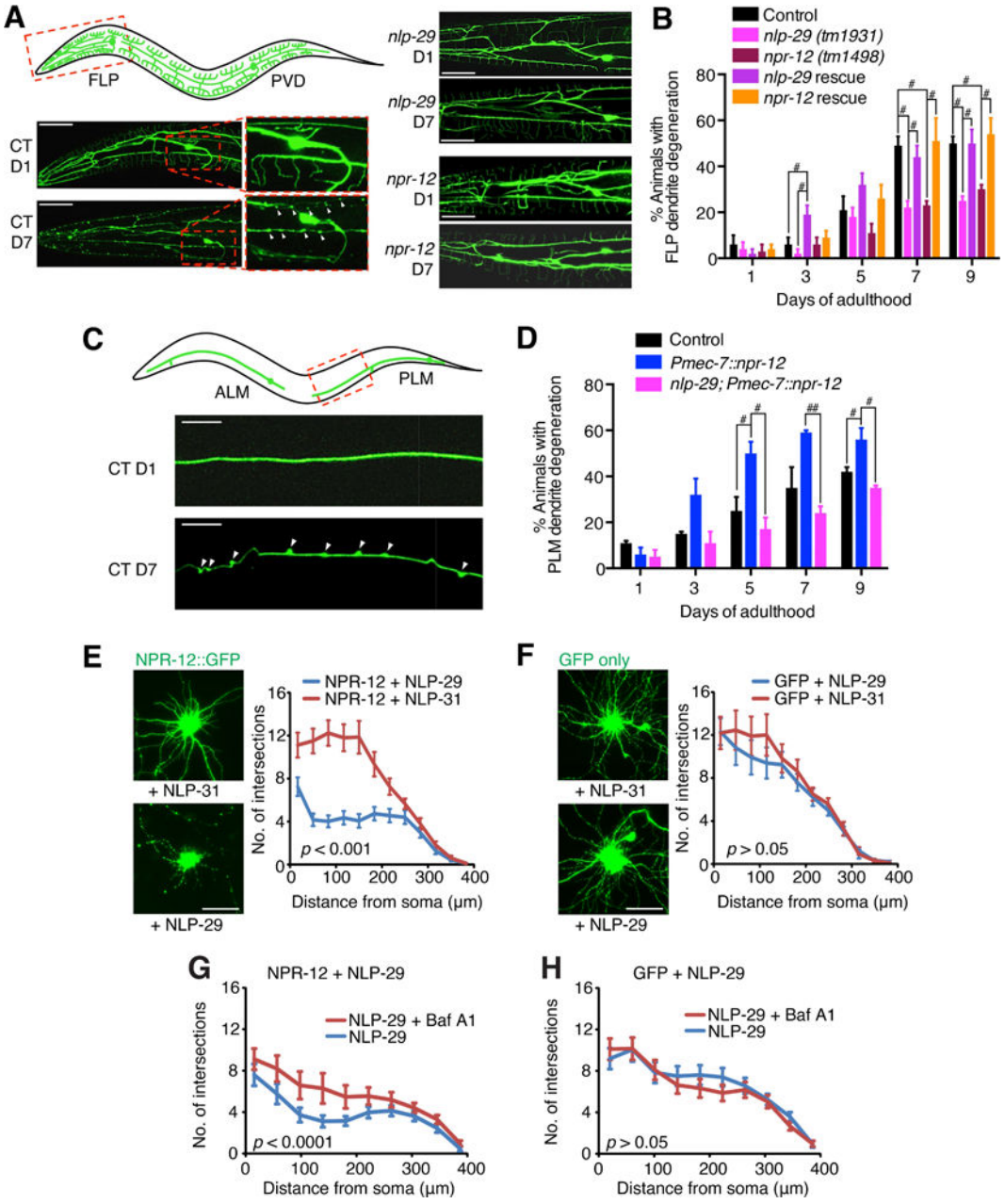

Figure 6. NLP-29 and NPR-12 regulate dendrite degeneration in other *C. elegans* and mammalian neurons

(A) Representative images of FLP dendrite degeneration in control animals [*yadEx650* (*Pmec-3::GFP*)], *nlp-29(lf) (tm1931;yadEx650)*, and *npr-12(lf) (tm1498;yadEx650)* during aging. White arrows: typical bead or bubble-like structures. Scale bars: 50 μm. CT, control. **(B)** FLP dendrite degeneration in control, *nlp-29(tm1931)*, *npr-12(tm1498)* and transgenic rescue strains. The *col-19* promoter was used for epidermis-specific rescue of *nlp-29*, and the *mec-7* promoter was used for cell-autonomous rescue of *npr-12*. Data were analyzed by one-way ANOVA, followed by Fisher's LSD post-hoc test, for each day. # $p < 0.05$. No difference was detected between *nlp-29* and *npr-12* mutants at any time point.

(C) Representative images of degeneration of PLM sensory processes/dendrites in control animals [*zdIs5* (*Pmec-4::GFP*), CT] during aging. White arrows: typical bead or bubble-like structures. Scale bars: 20 μm.

(D) Degeneration of PLM sensory processes/dendrites in control animals, animals with ectopic expression of *npr-12* in PLM neurons driven by the *mec-7* promoter (*Pmec-7::npr-12*), and *nlp-29(tm1931);Pmec-7::npr-12*. Data were analyzed by one-way ANOVA, followed by Fisher's LSD post-hoc test, for each day. # $p < 0.05$, ## $p < 0.001$.

(E) Rat cortical neurons expressing NPR-12::2A::GFP were either treated with 10 μM NLP-31 (control) or 10 μM NLP-29 peptides. Representative images are shown in the left panels. Scale bar = 10 μm. Sholl analysis of neurite complexity and continuity demonstrates that cortical neurons expressing NPR-12 treated with NLP-29 had significant degenerative dendritic morphology compared with NLP-31 treated neurons (n = 15 cells/condition). ANCOVA: $p < 0.001$.

(F) Rat cortical neurons expressing GFP only were either treated with 10 μM NLP-31 (control) or 10 μM NLP-29 peptides. Representative images are shown in the left panels. Scale bar = 10 μm. Sholl analysis demonstrates that no significant difference was found in dendritic morphology between NLP-29 and NLP-31 treatment in the absence of NPR-12. (n = 15 cells/condition). ANCOVA: $p > 0.05$.

(G–H) Rat cortical neurons expressing NPR-12::2A::GFP *(G)* or GFP only *(H)* were either treated with 10 μM NLP-29 peptides only or 10 μM NLP-29 peptides + 10 nM bafilomycin A1 (Baf A1). Sholl analysis of neurite complexity and continuity demonstrates that the autophagy inhibitor Baf A1 significantly suppressed the changes of dendritic morphology that were induced by NLP-29 treatment in NPR-12-expressing neurons. n = 26~29 cells/condition). ANCOVA was used to detect differences between NLP-29 and NLP-29 + Baf A1.

Data are represented as mean ± SEM. Non-significant comparisons are not indicated in the figure.

See also Figure S5 and Figure S6.

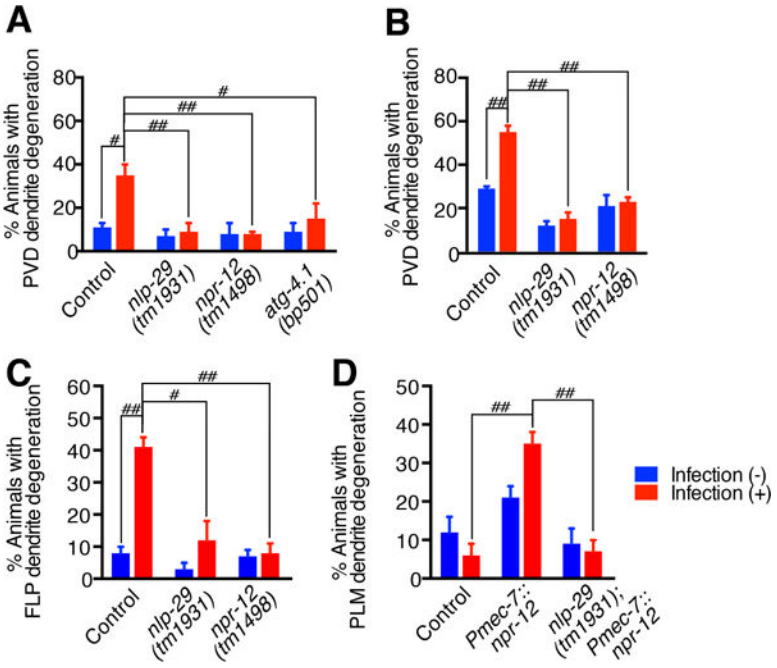

Figure 7. Fungal infection induces dendrite degeneration via NLP-29 and NPR-12

Animals were either treated with *Drechmeria coniospora* or vehicle solution (NaCl 50 mM), and were quantified for dendrite degeneration after 36-hour incubation in the pathogen or vehicle. The mean differences between each strain under different treatment conditions were analyzed by one-way ANOVA, followed by Fisher's LSD post-hoc test. **(A)** Effects of infection on PVD dendrite degeneration; animals were treated on Day 1. **(B)** Effects of infection on PVD dendrite degeneration; animals were treated on Day 3. **(C)** Effects of infection on FLP dendrite degeneration; animals were treated on Day 1. **(D)** Effects of infection on degeneration of PLM dendrite/sensory processes; animals were treated on Day 1; ectopic expression of *npr-12* in PLM neurons was driven by the *mec-7* promoter (*Pmec-7::npr-12*). # $p < 0.05$, ## $p < 0.001$.

Data are represented as mean ± SEM. Non-significant comparisons are not indicated in the figure.

See also Figure S7.